Chapter I

Diluted magnetic semiconductor quantum dots

This chapter aim to present the system we will study as well as the main theoretical tools one needs to understand it fully. We begin presenting the semiconductors and their electronic structure, and how the strains affect it. We then reduce the dimensions of the system we look at to get to one of the core of this thesis: the quantum dot (QD). We first see how the confinement affect the carriers energies, and we then study the QD optical properties, detailing the effects of the carrier exchange interaction and the anisotropy of the strains in the QD on its emission.

In the next sections, we open the discussion on the magnetic atoms, starting with the Diluted Magnetic Semiconductors, semiconductors with a low density of magnetic impurity inserted in the lattice. We see how these impurities can dramatically change the behaviour of the carriers and thus the properties of said semiconductor. We then give more details on the two atoms we focus on in this thesis: the Manganese and the Chromium. The second section details their interactions with the carriers, while we study in the third their interaction with the semiconductor crystal field.

Finally, we give a simple example of application for these theories, studying a simple system: an exciton and a single Manganese atom in a quantum dot.

I.1 II-VI semiconductor quantum dots

I.1.1 Band structure of CdTe/ZnTe

CdTe and ZnTe are two II-VI semiconductors, meaning they are composed of an anion from the column VI of periodic table (Te), and a cation from the column II (Cd or Zn). They both crystallize in a zinc blend structure when grown in Molec-

ular Beam Epitaxy (MBE, see Chap. ?? for more informations on this technique). As shown in Fig. I.1, in this structure, each species is organized in a face centred lattice, one them being shift from the other by a quarter of the [111] diagonal. Each ion is then in a tetragonal environment, meaning the zinc-blende structure is of the T_d space-group.

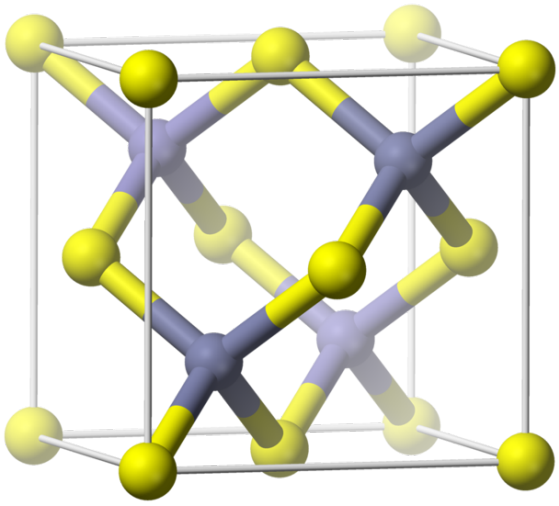

Figure I.1: Zinc-blende crystal elementary cell. Both CdTe and ZnTe crystallize in this structure.

The external orbitals are s for the cation ($4d^{10}5s^2$ for Cd, $3d^{10}4s^2$ for Zn) and p for the anion ($4d^{10}5s^25p^4$ for Te). Considering a N units crystal, it then contain 8N valence electrons, coming from the s and p levels of the ions. The s and p orbitals of these atoms hybridize to form 8 levels, 4 bonding and 4 anti-bonding.

The lowest band of the bonding levels, coming from s orbitals, will be filled by 2N valence electrons. 6N will be taken to fill the three bonding bands of higher energy, formed by the hybridization of p orbitals. Those bonding states form the valence band. At higher energy, the anti-bonding states form the conduction band. Since all the available electrons are used to fill the valence band, the conduction band is empty in the ground state. The lower energy band of the conduction band is formed by the anti-symmetric combination of the s orbitals. At higher energy, the anti-symmetric hybridization of p orbitals form three other bands.

The energy needed to promote one electron from the higher energy state of the valence band to the lower energy state of the conduction band is called the gap. In the ZnTe and CdTe cases, they are equal to $E_{g,ZnTe} = 2.40$ eV and $E_{g,CdTe} = 1.60$ eV at 5K [1]. It is possible to promote an electron from the valence band to the conduction band by injecting in the semiconductor at least as much energy as the

size of the gap. This absence of an electron in the valence band can be viewed as a quasi-particle called a hole, with a spin and a charge opposed to the one of the promoted electron.

Introducing the spin-orbit interaction, the conduction band, formed by the hybridization of s orbitals, is of Γ_6 (spherical) symmetry at the center of the Brillouin zone (for $k \simeq 0$), two-fold degenerated, with an orbital momentum (spin) $\sigma = \frac{1}{2}$. In a similar fashion, the valence band will be split into two bands: a first one of Γ_8 symmetry, with a spin $J = \frac{3}{2}$, four-fold degenerated ; and the second one, at lower energy, of Γ_7 symmetry, with a spin $\frac{1}{2}$, two-fold degenerated. The splitting $\Gamma_7 - \Gamma_8$ is of $\Delta_{SO} \simeq 0.9$ eV in II-VI semiconductor. This gap is wide enough to ignore the effect of the Γ_7 band for the rest of this document and focusing on the effect between the top of the valence band and the bottom of the conduction band.

Since the conduction band has a spin $\frac{1}{2}$, we can write it using Pauli matrix, defining the following operators:

$$\sigma_x = \frac{1}{2}\begin{pmatrix} 0 & 1 \\ 1 & 0 \end{pmatrix} \quad ; \quad \sigma_y = \frac{1}{2}\begin{pmatrix} 0 & -i \\ i & 0 \end{pmatrix} \quad ; \quad \sigma_z = \frac{1}{2}\begin{pmatrix} 1 & 0 \\ 0 & -1 \end{pmatrix} \tag{I.1}$$

In the same fashion, we can define the spin operators in the top of the valence band. For spin a $\frac{3}{2}$, we have:

$$J_x = \begin{pmatrix} 0 & \frac{\sqrt{3}}{2} & 0 & 0 \\ \frac{\sqrt{3}}{2} & 0 & 1 & 0 \\ 0 & 1 & 0 & \frac{\sqrt{3}}{2} \\ 0 & 0 & \frac{\sqrt{3}}{2} & 0 \end{pmatrix} \quad ; \quad J_y = \begin{pmatrix} 0 & -\frac{i\sqrt{3}}{2} & 0 & 0 \\ \frac{i\sqrt{3}}{2} & 0 & -i & 0 \\ 0 & i & 0 & -\frac{i\sqrt{3}}{2} \\ 0 & 0 & \frac{i\sqrt{3}}{2} & 0 \end{pmatrix}$$
$$J_z = \begin{pmatrix} \frac{3}{2} & 0 & 0 & 0 \\ 0 & \frac{1}{2} & 0 & 0 \\ 0 & 0 & -\frac{1}{2} & 0 \\ 0 & 0 & 0 & -\frac{3}{2} \end{pmatrix} \tag{I.2}$$

Finally, for any spin operator O ($O = \boldsymbol{\sigma}$, $\mathbf{J}$ or any other spin operator of this document), we can define the ladder operator, flipping the considered spin by one unit, such as $O_+|O\rangle \propto |O+1\rangle$ and $O_-|O\rangle \propto |O-1\rangle$. They write in the general case as:

$$O_+ = O_x + iO_y \tag{I.3}$$
$$O_- = O_x - iO_y \tag{I.4}$$

The whole CdTe band structure is presented on Fig. I.2. One can note that CdTe is a direct gap semiconductor: the highest energy point of the valence band

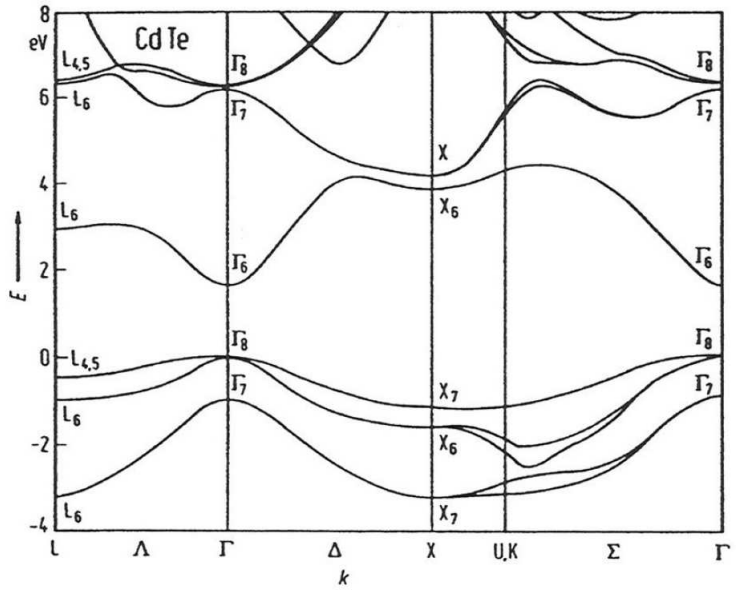

Figure I.2: CdTe band structure

correspond to the lowest energy point of the conduction band, in Γ. Near the band edge, we can describe the curvature of the energy $E(\mathbf{k})$ of the band using an effective mass for the carrier on it:

$$E_{\{c,v\}}(\mathbf{k}) = -\frac{(\hbar k)^2}{2m_{\{c,v\}}(\mathbf{k})} \tag{I.5}$$

As we move away from the Γ point, the valence band into split two branches: the one with small curvature, meaning a high effective mass for the carriers on it, is called the heavy-hole (hh) band, while the one presenting the highest curvature and smallest effective mass is called the light-hole (lh) band.

One way to understand this evolution is to apply the **k**.**p** approximation, as proposed by Kane in 1957 [2]. This model gives an estimation of the electronic band structure starting from the exact solution and energy of the Schrödinger equation at the center of the Brillouin. The hamiltonian to resolve is then :

$$\left(\frac{p^2}{2m_0} + U(\mathbf{r})\right)|\psi_{n,\mathbf{k}}\rangle = E_{n,\mathbf{k}}|\psi_{n,\mathbf{k}}\rangle \tag{I.6}$$

with $U(\mathbf{r})$ the potential of the crystal, m_0 the mass of a free carrier and $|\psi_{n,\mathbf{k}}\rangle$ the Bloch wave, separated between a periodic part $u_{n,\mathbf{k}}(\mathbf{r})$ and plane-wave part $\exp(i\mathbf{k}.\mathbf{r})$ as follow :

$$|\psi_{n,\mathbf{k}}\rangle = u_{n,\mathbf{k}}(\mathbf{r})\exp(i\mathbf{k}.\mathbf{r}) \tag{I.7}$$

We solve this hamiltonian for carrier on the Γ_6 and Γ_8 bands. The z-axis is defined along the growth direction of the semiconductor and chosen as the quantization axis. The resolution was done in detail in Claire Le Gall PhD thesis [3]. We then find the energies:

$$\begin{aligned} E_c(k_z) &= E_c + \frac{\hbar^2 k_z^2}{2m_c} \\ E_{v,\pm\frac{1}{2}}(k_z) &= E_v - \frac{\hbar^2 k_z^2}{2m_{lh}} \\ E_{v,\pm\frac{3}{2}}(k_z) &= E_v + \frac{\hbar^2 k_z^2}{2m_0} \end{aligned} \tag{I.8}$$

with E_c (respectively, E_v) the energy of the conduction band (respectively, the valence band), m_c the effective mass of the carrier in the conduction band and m_{lh} the effective mass of the light hole. One can see that the splitting of the valence band separate the carrier with a spin $J_z = \pm\frac{3}{2}$ (hh) from the one with a spin $J_z = \pm\frac{1}{2}$ (lh). However, neglecting the bands other than Γ_6 and Γ_8 leads to a positive curvature for the hh. To correct this problem, we would have to take into account higher energies conduction bands, which will repel the hh band and give it its negative curvature.

Another solution to have the matrix describing the Γ_8 band is to use symmetry consideration. Luttinger showed in 1956 [4] that the only Hamiltonian fulfilling the cubic symmetry is:

$$\mathcal{H}_L = -\frac{h^2}{2m_0}\left(\gamma_1 k^2 I_4 - 2\gamma_2 \sum_i k_i^2 \left(J_i^2 - \frac{1}{3}J^2\right) - 2\gamma_3(k_x k_y(J_x J_y + J_y J_x) + c.p.)\right) \tag{I.9}$$

with γ_1, γ_2 and γ_3 the Luttinger parameters, I_4 the 4×4 identity matrix, $\mathbf{k}$ a vector of the Brillouin zone, $\mathbf{J}$ the orbital momentum operator with J_x, J_y and J_z being 4×4 matric satisfying $[J_x, J_y] = iJ_z$ and circular permutation ($c.p$). This hamiltonian can be simplified using the parameters:

$$\begin{aligned} A &= \gamma_1 + \frac{5}{2}\gamma_2 \\ B &= 2\gamma_2 \\ C &= 2(\gamma_3 - \gamma_2) \end{aligned} \tag{I.10}$$

The Luttinger hamiltonian can then be rewritten:

$$\mathcal{H}_L = -\frac{h^2}{2m_0}(Ak^2 I_4 - B(\mathbf{k}.\mathbf{J})^2 + C(k_x k_y(J_x J_y + J_y J_x) + c.p.)) \tag{I.11}$$

Table I.1: Physical parameters for CdTe and ZnTe.

	CdTe	ZnTe
E_g	1606 meV	2391 meV
ε_r	10.6	9.7
a_0	6.48 Å	6.10 Å
Δ_{SO}	0.90 eV	0.91 eV
γ_1	4.8	4.07
γ_2	1.5	0.78
γ_3	1.9	1.59
$m_{hh,z}$	0.556	0.398
$m_{hh,\perp}$	0.159	0.206
$m_{lh,z}$	0.128	0.178
$m_{lh,\perp}$	0.303	0.303
m_e	0.096	0.116

The B-term lifts the degeneracy of the Γ_8 band into two sub-bands as shown above, and is invariant under arbitrary rotations. The C-term describes the warping of the valence band.

In the spherical approximation, the Luttinger hamiltonian has two eigenvalues, giving us the value of the lh and hh effective mass:

$$\begin{aligned} E_{hh} &= -\frac{\hbar^2 k^2}{2m_0(A-2.25B)^{-1}} = -\frac{\hbar^2 k^2}{2m_0(\gamma_1-2\gamma_2)^{-1}} = -\frac{\hbar^2 k^2}{2m_{hh}} \\ E_{lh} &= -\frac{\hbar^2 k^2}{2m_0(A-0.25B)^{-1}} = -\frac{\hbar^2 k^2}{2m_0(\gamma_1+2\gamma_2)^{-1}} = -\frac{\hbar^2 k^2}{2m_{lh}} \end{aligned} \tag{I.12}$$

As expected from the band structure, the hh presents a negative curvature.

The parameters and carriers effective masses are given in the Tab. I.1.1.

The Luttinger hamiltonian is usually written in matrix form. In the ($u_{\Gamma_8,+\frac{3}{2}}$, $u_{\Gamma_8,+\frac{1}{2}}$, $u_{\Gamma_8,-\frac{1}{2}}$, $u_{\Gamma_8,-\frac{3}{2}}$) basis, we can rewrite it:

$$\mathcal{H}_L = -\frac{\hbar^2}{2m_0}\begin{pmatrix} a_{hh} & b_{Lutt} & c_{Lutt} & 0 \\ b^*_{Lutt} & a_{lh} & 0 & c_{Lutt} \\ c^*_{Lutt} & 0 & a_{lh} & -b_{Lutt} \\ 0 & c^*_{Lutt} & -b^*_{Lutt} & a_{hh} \end{pmatrix} \tag{I.13}$$

with:

$$\begin{aligned} a_{hh} &= (\gamma_1 - 2\gamma_2)k_z^2 + (\gamma_1 + \gamma_2)k_\parallel^2 \\ a_{lh} &= (\gamma_1 + 2\gamma_2)k_z^2 + (\gamma_1 - \gamma_2)k_\parallel^2 \\ b_{Lutt} &= -2\sqrt{3}\gamma_3(k_x - ik_y)k_z \\ c_{Lutt} &= -\sqrt{3}(\gamma_2(k_x^2 - k_y^2) - 2i\gamma_3 k_x k_y) \end{aligned}$$

I.1.2 Lattice mismatch and the Bir-Pikus Hamiltonian

ZnTe crystal has a lattice parameter of $a_{ZnTe} = 6.10$ Å, while CdTe one is of $a_{CdTe} = 6.48$ Å. This lattice mismatch results in stress in a CdTe layer grown on a ZnTe substrate:

$$\varepsilon_\parallel = \frac{a_{ZnTe} - a_{CdTe}}{a_{CdTe}} = -5.8\% \tag{I.14}$$

In order to represent this strain and see its effects on the bands, we need to define a hamiltonian representing them. Strains deform the structure, so let's begin the representation with an volume $V = x\mathbf{u_x} + y\mathbf{u_y} + z\mathbf{u_z}$, with $(\mathbf{u_x}, \mathbf{u_y}, \mathbf{u_z})$ an orthonormal basis. This volume will transform into another one $V' = x\mathbf{u'_x} + y\mathbf{u'_y} + z\mathbf{u'_z}$, where:

$$\begin{aligned} \mathbf{u'_x} &= (1 + \varepsilon'_{xx})\mathbf{u_x} + \varepsilon'_{xy}\mathbf{u_y} + \varepsilon'_{xz}\mathbf{u_z} \\ \mathbf{u'_y} &= \varepsilon'_{yx}\mathbf{u_x} + (1 + \varepsilon'_{yy})\mathbf{u_y} + \varepsilon'_{yz}\mathbf{u_z} \\ \mathbf{u'_z} &= \varepsilon'_{zx}\mathbf{u_x} + \varepsilon'_{zy}\mathbf{u_y} + (1 + \varepsilon'_{zz})\mathbf{u_z} \end{aligned} \tag{I.15}$$

ε'_{ij} represents an expansion of the vector i in the direction j. They are small deformation of the lattice, so we choose $|\varepsilon'_{ij}| \ll 1$. Such transformation can be decomposed in a symmetric part, the strain tensor, and an antisymetric one. We note the strain tensor $\overline{\overline{\varepsilon}}$, defined such as:

$$\varepsilon_{ii} = \varepsilon'_{ii} \tag{I.16}$$

$$\varepsilon_{ij} = \frac{1}{2}\left(\varepsilon'_{ij} + \varepsilon'_{ji}\right) \tag{I.17}$$

In the linear regime, the strain tensor $\overline{\overline{\varepsilon}}$ is proportional to the stress tensor $\overline{\overline{\sigma}}$, where σ_{ij} describe a force parallel to i applied on a surface perpendicular to j. Therefore, σ_{ii} will describe an elongation or compression stress, while σ_{ij} $(i \neq j)$ represents a shear stress. Since these tensor are symmetric, we can reduce the number of coefficient from nine to six: σ_{xx}, σ_{yy}, σ_{zz}, $\sigma_{xy} = \sigma_{yx}$, $\sigma_{xz} = \sigma_{zx}$ and

$\sigma_{yz} = \sigma_{zy}$. Therefore, in the linear regime and for a cubic crystal, we can write the Hooke's law:

$$\begin{bmatrix} \sigma_{xx} \\ \sigma_{yy} \\ \sigma_{zz} \\ \sigma_{xy} \\ \sigma_{xz} \\ \sigma_{yz} \end{bmatrix} = \begin{bmatrix} C_{11} & C_{12} & C_{12} & 0 & 0 & 0 \\ C_{12} & C_{11} & C_{12} & 0 & 0 & 0 \\ C_{12} & C_{12} & C_{11} & 0 & 0 & 0 \\ 0 & 0 & 0 & 2C_{44} & 0 & 0 \\ 0 & 0 & 0 & 0 & 2C_{44} & 0 \\ 0 & 0 & 0 & 0 & 0 & 2C_{44} \end{bmatrix} \begin{bmatrix} \varepsilon_{xx} \\ \varepsilon_{yy} \\ \varepsilon_{zz} \\ \varepsilon_{xy} \\ \varepsilon_{xz} \\ \varepsilon_{yz} \end{bmatrix} \tag{I.18}$$

Since x, y and z are physically equivalent, as well as xy, xz and yz, only two diagonal coefficient are needed, C_{11} and C_{44}. These coefficient coupling strains in a direction to a force in the same direction are obviously positives.

When the considered cube is compressed in one direction (e.g. $\varepsilon_{zz} < 0$), it will expand in the other direction in order to minimize elastic energy (ε_{xx}, $\varepsilon_{yy} > 0$ in the example). If we don't allow strain in these other directions ($\varepsilon_{xx} = \varepsilon_{yy} = 0$), a stress in the x and y directions had to be applied to keep the cube from expanding in these directions (σ_{xx}, $\sigma_{yy} < 0$ in the example). We can therefore physically expect $C_{12} > 0$.

The strain hamiltonian can be constructed noticing that the strain tensor $\overline{\overline{\varepsilon}}$ induces a shift in the bands energy, and that any ε_{ij} has the same symmetry as $k_i k_j$. The hamiltonian should then be formarly identical to the Luttinger hamiltonian. In the Γ_8 subspace, we can then use the Luttinger Hamiltonian, written in Eq. I.9, replacing the $k_i k_j$ by ε_{ij}. We obtain the Bir-Pikus Hamiltonian by replacing the γ_j parameters by the Bir-Pikus parameters a_ν, b_{BP} and d_{BP} [5]:

$$\mathcal{H}_{BP} = a_\nu \sum_i \varepsilon_{ii} + b_{BP} \sum_i \varepsilon_{ii} \left(J_i^2 - \frac{1}{3} J^2 \right) + \frac{2 d_{BP}}{\sqrt{3}} \sum_{i>j} \varepsilon_{ij} \{ J_i J_j \} \tag{I.19}$$

with $\varepsilon = Tr(\overline{\overline{\varepsilon}}) = \varepsilon_{xx} + \varepsilon_{yy} + \varepsilon_{zz}$ and $\{J_i J_j\} = \frac{1}{2}(J_i J_j + J_j J_i)$

The a_ν term, called the hydrostatic term, shifts the Γ_8 energy. The b_{BP} term represents the shear strain. In case of non-equal ε_{ii}, its effect is to lift up the two Γ_8 sub-bands as did a $k \neq 0$ in the Luttinger hamiltonian. The d_{BP} term, the pure shear strain (i.e ε_{ij} with $i \neq j$), has the same effect on the Γ_8 band.

One can notice that the Bir-Pikus hamiltonian is completely independant from $\mathbf{k}$, meaning that the band hamiltonian of a strain semiconductor is simply the sum of the Luttinger hamiltonian $\mathcal{H}_L$ (Eq. I.9) and the Bir-Pikus hamiltonian $\mathcal{H}_{BP}$ (Eq. I.19).

Let see how this apply to a CdTe layer deposited on a ZnTe layer. As previously, we define z as the growth direction. As shown at the begin of this part, CdTe and ZnTe have a lattice mismatch of 5.8%. Since both crystallize in a cubic lattice,

the strains are the same in the x and y direction. We can then write the strains in the xy plane:

$$\varepsilon_{xx} = \varepsilon_{yy} = \varepsilon_{\parallel} = \frac{a_{ZnTe} - a_{CdTe}}{a_{CdTe}} \tag{I.20}$$

In the z direction, however, no stress applies: the crystal is free to expand in this direction in order to reduce the elastic energy. Therefore, we can write $\sigma_{zz} = 0$ and, according to Hooke's law in Eq. I.18:

$$\begin{aligned} \sigma_{zz} &= C_{12}\varepsilon_{xx} + C_{12}\varepsilon_{yy} + C_{11}\varepsilon_{zz} \\ &= 0 \end{aligned} \tag{I.21}$$

Using equality I.20, we can then deduce:

$$\varepsilon_{zz} = -\frac{2C_{12}}{C_{11}}\varepsilon_{\parallel} = -\frac{2C_{12}}{C_{11}}\frac{a_{ZnTe} - a_{CdTe}}{a_{CdTe}} \tag{I.22}$$

Since we grow CdTe over a ZnTe substrate, the CdTe lattice is compressed in the plane, i.e. $\varepsilon_{\parallel} < 0$. Since C_{11}, $C_{12} > 0$ and $\varepsilon_{\parallel} < 0$ for CdTe over ZnTe (see Eq. I.20), one can easily deduce that $\varepsilon_{zz} > 0$. In the hypothesis of no defect created by the lattice mismatch, all the other strain terms are equal to zero. We can then decompose this strain into two component: a hydrostatic part describing the volume variation without breaking the cubic symmetry, and a shear part introducing an anisotropy, breaking this symmetry:

$$\overline{\overline{\varepsilon_{hyd}}} = \frac{1}{3}(\varepsilon_{xx} + \varepsilon_{yy} + \varepsilon_{zz})I_3 \tag{I.23}$$

$$\overline{\overline{\varepsilon_{sh}}} = \overline{\overline{\varepsilon}} - \overline{\overline{\varepsilon_{hyd}}} \tag{I.24}$$

One can notice that $Tr(\overline{\overline{\varepsilon_{hyd}}}) = Tr(\overline{\overline{\varepsilon}}) = \varepsilon$. Since in the case of a hydrostatic compression, such as what is the case with CdTe over ZnTe, $\varepsilon_{hyd} < 0$, we then have $\varepsilon < 0$ and, according to the Bir-Pikus hamiltonian (Eq. I.19), the gap of CdTe increase. For CdTe, Bir-Pikus parameter are $a_\nu = 0.91$ eV, $b_{BP} = 0.99$ eV and $d_{BP} = 2.76$ eV [6].

Seeing that $\varepsilon_{ij} = 0$ for $i \neq j$, we can rewrite the Bir-Pikus hamiltonian without the shear strain term. Moreover, since $J^2 = J_x^2 + J_y^2 + J_z^2$ and that $\varepsilon_{xx} = \varepsilon_{yy} = \varepsilon_{\parallel}$, we can simplify this hamiltonian to:

$$\mathcal{H}_{BP,biax} = a_\nu \varepsilon I_4 + \frac{b_{BP}}{3}(\varepsilon_{\parallel} - \varepsilon_{zz})(J_x^2 + J_y^2 - 2J_z^2) \tag{I.25}$$

And, since we are in the valence band with $J = \frac{3}{2}$ and $J_x^2 + J_y^2 + J_z^2 = J(J+1)I_4$, we can simplify the Bir-Pikus hamiltonian to its final form in the case of biaxal strain:

$$\mathcal{H}_{BP,biax} = \left(a_\nu \varepsilon + \frac{5}{4} b_{BP}(\varepsilon_{\parallel} - \varepsilon_{zz})\right) I_4 - b_{BP}(\varepsilon_{\parallel} - \varepsilon_{zz})J_z^2 \tag{I.26}$$

Using Eq. I.20 and I.22, we can easily calculate $\varepsilon_{\parallel} - \varepsilon_{zz}$. Since $J_z|n\rangle = n|n\rangle$, we find:

$$\begin{aligned} E_{\pm\frac{3}{2}} - E_{\pm\frac{1}{2}} &= -2b_{BP}\left(1 + \frac{2C_{12}}{C_{11}}\right)\frac{a_{ZnTe} - a_{CdTe}}{a_{CdTe}} \\ &= 2b_{BP}\left(1 + \frac{2C_{12}}{C_{11}}\right)\frac{a_{CdTe} - a_{ZnTe}}{a_{CdTe}} \end{aligned} \tag{I.27}$$

We find that, in a fully strained CdTe layer over a ZnTe substrate, the hh band is 300 meV above the lh one. In first approximation, we can then neglect the lh contribution in these nanostructures.

I.1.3 3D confinement: the quantum dot

Embedding a semiconductor in another one of larger gap creates trap for carriers, confining them in one or multiple directions. CdTe conduction band is at a lower energy than ZnTe ones, creating such a trap. Using the procedure described in Chap. **??**, we can create nanometre size island of CdTe in a ZnTe lattice, effectively confining electrons in all three directions, acting like a 3D trap for the free carriers. This lead to a quantization of the carriers energy levels and a discretization of the optical properties. This confinement being analogue to the Coulomb interaction of an isolated atom, such a structure is often dubbed "artificial atom". However, the interaction between the hole and the electron cannot be overlook, adding to this potential the Coulomb interaction between the particule and the quasi-particule. It consists of an attractive term, shifting energy levels, and an exchange interaction (discussed in Sec. I.1.4). Moreover, the hole being the absence of an electron, its energy, charge, spin, orbital momentum, $\mathbf{k}$ and mass are, by definition, opposite to the missing electron. The electron-hole system has a hydrogen-like behaviour and is called an exciton.

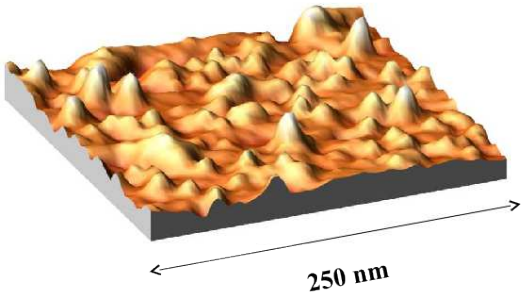

Figure I.3: AFM image (AFM image (250 nm × 250 nm) of CdTe/ZnTe quantum dots before caping. The dot density is estimated to be in the 10^{10} dots.cm^{-2} range.

Before studying in more detail the exchange interaction between the hole and the electron, we will see the optical properties of this system. In order to do so,

we develop the carrier wave-function on all the Bloch states:

$$\Psi(\mathbf{r}) = \sum_{n,\mathbf{k}} c_{n,\mathbf{k}} \psi_{n,\mathbf{k}} = \sum_{n,\mathbf{k}} c_{n,\mathbf{k}} u_{n,\mathbf{k}}(\mathbf{r}) \exp(i\mathbf{k}.\mathbf{r}) \tag{I.28}$$

Since we are in a confined environment, we can consider only the states around $\mathbf{k} = 0$. Since we consider the band extrema, we neglect for this part the inter-band wave function mixing and use the effective-mass approximation. We can then limit the expansion of Bloch state to an expansion on the $u_{n,0}(\mathbf{r}) \exp(i\mathbf{k}.\mathbf{r})$, with $n = \Gamma_6$ for the conduction band and $n = \Gamma_8$ for the valence. We can then write:

$$\Psi_c(\mathbf{r}) \simeq \sum_{\mathbf{k}} c_{\mathbf{k}} u_{\Gamma_6,0}(\mathbf{r}) \exp(i\mathbf{k}.\mathbf{r}) = F_e(\mathbf{r}) u_{\Gamma_6,0} \tag{I.29}$$

$$\Psi_v(\mathbf{r}) \simeq \sum_{J_z=\{\pm\frac{3}{2},\pm\frac{1}{2}\},k} c_{J_z,\mathbf{k}} u_{\Gamma_8,J_z}(\mathbf{r}) \exp(i\mathbf{k}.\mathbf{r}) = \sum_{J_z=\{\pm\frac{3}{2},\pm\frac{1}{2}\}} F_{J_z}(\mathbf{r}) u_{\Gamma_8,J_z} \tag{I.30}$$

with $F_e(\mathbf{r}) = \sum_{\mathbf{k}} c_{\mathbf{k}} \exp(i\mathbf{k}.\mathbf{r})$ the electron envelop function and $F_{J_z}(\mathbf{r}) = c_{J_z,\mathbf{k}} \exp(i\mathbf{k}.\mathbf{r})$, $J_z = \{\pm\frac{3}{2}, \pm\frac{1}{2}\}$ the hole envelop functions.

The effective mass approximation allows us to replace the periodic crystal potential and the free-electron kinetic energy by the effective Hamiltonian representing the band extrema, using m_e for the conduction band and $\mathcal{H}_L + \mathcal{H}_{BP}$ for the top of the valence band. Considering the effective mass is the same in CdTe and ZnTe, we can now work with the simple picture of an effective mass carrier with the envelop function defined in Eqs. I.29 and I.30, trapped in a potential $V_e(\mathbf{r})$ for the conduction band or $V_h(\mathbf{r})$ for the valence band, created by the band offset between the two semiconductors. We write the Schrödinger equations for these particles:

$$\left(\frac{\hbar^2}{2m_e}\Delta\right) F_e(\mathbf{r}) + V_e(\mathbf{r}) F_e(\mathbf{r}) = E_e F_e(\mathbf{r}) \tag{I.31}$$

$$(\tilde{\mathcal{H}}_L + \tilde{\mathcal{H}}_{BP} + V_h(\mathbf{r})) \begin{pmatrix} F_{+\frac{3}{2}}(\mathbf{r}) \\ F_{+\frac{1}{2}}(\mathbf{r}) \\ F_{-\frac{1}{2}}(\mathbf{r}) \\ F_{-\frac{3}{2}}(\mathbf{r}) \end{pmatrix} = E_h \begin{pmatrix} F_{+\frac{3}{2}}(\mathbf{r}) \\ F_{+\frac{1}{2}}(\mathbf{r}) \\ F_{-\frac{1}{2}}(\mathbf{r}) \\ F_{-\frac{3}{2}}(\mathbf{r}) \end{pmatrix} \tag{I.32}$$

with $\tilde{\mathcal{H}}_L$ and $\tilde{\mathcal{H}}_{BP}$ the hole hamiltonians, opposite to the electron hamiltonians defined in Eq. I.9 and I.19. In $\tilde{\mathcal{H}}_L$, the k-terms transform into a gradient of the envelop function with the form $i\nabla$. For simplicity, the $\tilde{}$ will be dropped in the next equations. The derivation of the effective mass approximation can be found in reference [7].

As pointed out in the end of Sec. I.1.2, the gap between lh and hh is wide enough to neglect lh contribution in first approximation. This is called the heavy

hole approximation, uncoupling the four differential equations defined in Eq. I.32. Only the ground states $|\pm\frac{3}{2}\rangle$ are considered, with the effective mass given by the diagonal term of $\mathcal{H}_L$, noted $m_{h,\parallel}$ in the plane and $m_{h,z}$ along the growth axis. The spin operator J_x, J_y and J_z can then be redefined in the heavy-hole space as j_x, j_y, j_z, written with the Pauli matrix looking like σ_x, σ_y and σ_z.

Even with those two approximations, this problem is still unsolvable analytically. However, it is possible for some chosen potentials. Let's consider a lens like quantum dot, with a radius in the xy plane, noted ρ, much larger than its height L_z. We can therefore define two different harmonic oscillators: a 2D oscillator $V_{c,v}(\rho)$ in the plane, and a 1D oscillator $V_{c,v}(z)$ along the growth axis:

$$V_{c,v}(\rho) = 4\Delta E_{c,v}\frac{\rho^2}{L_z^2} \tag{I.33}$$

$$V_{c,v}(z) = 4\Delta E_{c,v}\frac{z^2}{L_z^2} \tag{I.34}$$

with $\Delta E_{c,v}$ the difference of conduction (resp. valence) band energy between the two semiconductors. The potential of the whole quantum dot will the be $V_{c,v}(\mathbf{r}) = V_{c,v}(\rho)+V_{c,v}(z)$. Separating the potential in those two parts means we are searching for solution of the form $F(z,\rho,\theta) = \chi(z)\phi_{n,m}(\rho,\theta)$, with θ the angle between the position vector and the x axis.

We write the characteristic spatial width σ and characteristic frequency ω of the 2D harmonic oscillator felt by the hole:

$$\Sigma_\rho^h = \sqrt{\frac{\hbar}{m_{h,\parallel}\omega_\rho^h}} \tag{I.35}$$

$$\omega_\rho^h = \sqrt{\frac{8\Delta E_v}{m_{h,\parallel}L_\rho^2}} \tag{I.36}$$

We can write the same equality along z replacing ρ by z and $m_{h,\parallel}$ by $m_{h,z}$. The same can be done for electron, replacing the $m_{h,\parallel}$ or $m_{h,z}$ by m_e and E_v by E_c.

We can find in textbook such as ref. [8] the solution of a harmonic oscillator from which we can deduce the solution for the ground state (GS) and the first two degenerated excited states. The first excited state is found to have an angular momentum $l_z = \pm 1$, and is then noted $Exc, \pm 1$. The envelop functions and energy

are then found to be:

$$F_{c,v}^{GS}(z,\rho,\theta) = \frac{1}{(\sqrt{\pi}\Sigma_z)^{\frac{1}{2}}} \exp\left(-\frac{z^2}{2\Sigma_z^2}\right) \frac{1}{(\sqrt{\pi}\Sigma_\rho)^{\frac{1}{2}}} \exp\left(-\frac{\rho^2}{2\Sigma_\rho^2}\right) \tag{I.37}$$

$$E_{e,h}^{GS} = \hbar\frac{\omega_z^{e,h} + \omega_\rho^{e,h}}{2} \tag{I.38}$$

$$F_{c,v}^{Exc,\pm1}(z,\rho,\theta) = \frac{1}{(\sqrt{\pi}\Sigma_z)^{\frac{1}{2}}} \exp\left(-\frac{z^2}{2\Sigma_z^2}\right) \frac{1}{(\sqrt{\pi}\Sigma_\rho)^{\frac{1}{2}}} \exp\left(-\frac{\rho^2}{2\Sigma_\rho^2}\right) \frac{\rho}{\sigma_\rho} \exp(\pm i\theta) \tag{I.39}$$

$$E_{e,h}^{Exc,\pm1} = \hbar\frac{\omega_z^{e,h} + 3\omega_\rho^{e,h}}{2} \tag{I.40}$$

We see that these energy levels are quantified in a way looking like an isolated atom, as pointed earlier. In reference to the atomic notation, the ground state, lower energy level, is noted S and the two first degenerated level are noted P, even though atomic p-states usually are 3 fold degenerated.

One remarkable feature of the envelop functions is that both GS and the two first excited states present the same envelop along the z axis. The cause is directly the symmetry of the QD: since $L_z \ll L_\rho$, $\omega_z^{e,h} \gg \omega_\rho^{e,h}$, and since $E_{osc.\ harmo.} = (n+\frac{1}{2})\hbar\omega$, the next possible envelop function along the z axis is at higher energy than the next one in the plane. This geometry is also responsible for the 2 fold degeneracy of the P-states.

Both the GS and the excited states are once again degenerated due to the spin of the electron and the hole. The electron is in the conduction band with the Γ_6 symmetry: it can then take the value $\sigma_z = \pm\frac{1}{2}$ (noted $|\uparrow\rangle$ for $+\frac{1}{2}$ and $|\downarrow\rangle$ for $-\frac{1}{2}$). Since we are in the hh approximation, considering the lh are far enough from the band edge to be negligible, the hole spin can only take the values $J_z = \pm\frac{3}{2}$ (noted $|\Uparrow\rangle$ for $+\frac{3}{2}$ and $|\Downarrow\rangle$ for $-\frac{3}{2}$). As pointed ahead, the hole is defined with the opposed characteristic of the missing electron (which may not be the one trapped in the QD). For instance, a hole $|\Downarrow\rangle$ corresponds to the absence of a valence electron $\Psi_v(\mathbf{r}) = u_{\Gamma_8,\frac{3}{2}}(\mathbf{r})F_{\frac{3}{2}}(\mathbf{r})$.

In order to find the optical properties of the quantum dot, we use the dipole approximation, giving the coupling to light as $H = -\frac{q}{m}\mathbf{p}.\mathbf{A}$, with $\mathbf{p}$ the momentum and $\mathbf{A}$ the vector potential. We can then determine the optical properties looking at the coupling through the $\mathbf{p}$ operator. In a QD, the light-matter interaction occur mainly through two processes: the absorption of a photon creating an exciton, and the recombination of an exciton emitting a photon. To model this, we consider the interband matrix element between the two electronic states Ψ_c and Ψ_v, as written

in Eqs. I.29 and I.30:

$$|\langle\Psi_v|\mathbf{p}|\Psi_c\rangle|^2 = |\langle F_v|F_c\rangle|^2|\langle u_{\Gamma_8,J_z}|\mathbf{p}|u_{\Gamma_6,\sigma_z}\rangle|^2 \tag{I.41}$$

The first term is just the overlap of the envelop function, making sure the hole and the electron are of the right state: a transition between a P state of the valence band and a S state in the conduction band is then forbidden.

The second term, showing the interband matrix elements, depending only on the symmetry of the Bloch functions, will then draw the rule for the recombination. We use the notation define above to note the electron state in the conduction band. The valence band, formed by p atomic states, three times degenerated, can be written from the $|X\rangle$, $|Y\rangle$ and $|Z\rangle$ electronic states as follows:

$$|+1\rangle = -\frac{|X\rangle + i|Y\rangle}{\sqrt{2}} \tag{I.42}$$

$$|0\rangle = |Z\rangle \tag{I.43}$$

$$|-1\rangle = \frac{|X\rangle - i|Y\rangle}{\sqrt{2}} \tag{I.44}$$

We can now write the states of the conduction band by composing these electronic states to the spin states:

$$|u_{\Gamma_8,+\frac{3}{2}}\rangle = |+1\rangle|\uparrow\rangle \tag{I.45}$$

$$|u_{\Gamma_8,+\frac{1}{2}}\rangle = \sqrt{\frac{2}{3}}|0\rangle|\uparrow\rangle + \sqrt{\frac{1}{3}}|+1\rangle|\downarrow\rangle \tag{I.46}$$

$$|u_{\Gamma_8,-\frac{1}{2}}\rangle = \sqrt{\frac{2}{3}}|0\rangle|\downarrow\rangle + \sqrt{\frac{1}{3}}|-1\rangle|\uparrow\rangle \tag{I.47}$$

$$|u_{\Gamma_8,-\frac{3}{2}}\rangle = |-1\rangle|\downarrow\rangle \tag{I.48}$$

Since we are working in the hh approximation, we neglect the contribution of the states $|u_{\Gamma_8,\pm\frac{1}{2}}\rangle$, calculating the interband matrix element only for $|u_{\Gamma_8,\pm\frac{3}{2}}\rangle$. Since $|\uparrow\rangle$ and $|\downarrow\rangle$ are orthogonal states, it is then clear that there is only two optically active transitions:

- between $|u_{\Gamma_6,\uparrow}\rangle$ and $|u_{\Gamma_8,+\frac{3}{2}}\rangle$ (hole $|\Downarrow\rangle$), coupled by $p_- = p_x - ip_y$, corresponding to $\sigma-$ photon absorption or emission.
- between $|u_{\Gamma_6,\downarrow}\rangle$ and $|u_{\Gamma_8,-\frac{3}{2}}\rangle$ (hole $|\Uparrow\rangle$), coupled by $p_+ = p_x + ip_y$, corresponding to $\sigma+$ photon absorption or emission.

We see thus that, for an exciton in the S state of the QD, four configurations are possible. First, we have the bright states $|\uparrow\Downarrow\rangle$ for a $\sigma-$ absorption, with an

angular momentum $X_z = \sigma_z + j_z = \frac{1}{2} - \frac{3}{2} = -1$; and $|\downarrow\Uparrow\rangle$, for a $\sigma+$ absorption, with an angular momentum $X_z = -\frac{1}{2} + \frac{3}{2} = +1$. Both of these states are optically active, meaning their transitions are permitted and they can recombine radiatively. Two other states, not able to recombine radiatively, can exists and are called dark states: $|\uparrow\Uparrow\rangle$, with an angular momentum $X_z = +2$, and $|\downarrow\Downarrow\rangle$, with an angular momentum $X_z = -2$.

Approximating the QD potential as harmonic usually overestimate the confinement, and thus the single-particle energy. But the wave-functions found in this chapter can still be used as trial wave-functions for variational calculations in other potential, in order to estimate the correct energy level.

We discussed in this chapter about the neutral exciton (X), formed by a single electron-hole pair. However, several types of exciton can be observed in a quantum dots. First to consider are the charged excitons. In this case, a supplementary charge is injected in the QD in addition to the exciton, forming a hole-hole-electron (X^+) or hole-electron-electron (X^-) complex. It also happen that two excitons with opposed spins are trapped in a dot. This complex is called biexciton, noted X^2, and relax to leave a single neutral exciton in the QD. Charged biexciton and other multi-exciton complex also exist but are not discussed in this thesis. Even if the physics of each of this systems is different, the selection rules devised in this chapter apply to all of them.

I.1.4 Electron-hole exchange in quantum dots

An electron in the conduction band of a semiconductor interacts with all the electrons of the valence band. Solving such a system would be impossible. However, as shown in [9], we can treat this interaction as an interaction between this given electron and the corresponding hole, with a direct term and an exchange one. As classically expected from an electric interaction between two opposite charges, the direct Coulomb interaction is attractive and therefore lower the overall energy of the system. An electron in the conduction band of a semiconductor interacts with all the electrons of the valence band. Solving such a system would be impossible. However, as shown in [9], we can treat this interaction as an interaction between this given electron and the corresponding hole, with a direct term and an exchange one. As classically expected from an electric interaction between two opposite charges, the direct Coulomb interaction is attractive and therefore lower the overall energy of the system. An electron in the conduction band of a semiconductor interacts with all the electrons of the valence band. Solving such a system would be impossible. However, as shown in [9], we can treat this interaction as an interaction between this given electron and the corresponding hole, with a direct term and an exchange one. As classically expected from an electric interaction between two opposite charges, the direct Coulomb interaction is attractive and

therefore lower the overall energy of the system. An electron in the conduction band of a semiconductor interacts with all the electrons of the valence band. Solving such a system would be impossible. However, as shown in [9], we can treat this interaction as an interaction between this given electron and the corresponding hole, with a direct term and an exchange one. As classically expected from an electric interaction between two opposite charges, the direct Coulomb interaction is attractive and therefore lower the overall energy of the system. An electron in the conduction band of a semiconductor interacts with all the electrons of the valence band. Solving such a system would be impossible. However, as shown in [9], we can treat this interaction as an interaction between this given electron and the corresponding hole, with a direct term and an exchange one. As classically expected from an electric interaction between two opposite charges, the direct Coulomb interaction is attractive and therefore lower the overall energy of the system. An electron in the conduction band of a semiconductor interacts with all the electrons of the valence band. Solving such a system would be impossible. However, as shown in [9], we can treat this interaction as an interaction between this given electron and the corresponding hole, with a direct term and an exchange one. As classically expected from an electric interaction between two opposite charges, the direct Coulomb interaction is attractive and therefore lower the overall energy of the system. An electron in the conduction band of a semiconductor interacts with all the electrons of the valence band. Solving such a system would be impossible. However, as shown in [9], we can treat this interaction as an interaction between this given electron and the corresponding hole, with a direct term and an exchange one. As classically expected from an electric interaction between two opposite charges, the direct Coulomb interaction is attractive and therefore lower the overall energy of the system. An electron in the conduction band of a semiconductor interacts with all the electrons of the valence band. Solving such a system would be impossible. However, as shown in [9], we can treat this interaction as an interaction between this given electron and the corresponding hole, with a direct term and an exchange one. As classically expected from an electric interaction between two opposite charges, the direct Coulomb interaction is attractive and therefore lower the overall energy of the system. An electron in the conduction band of a semiconductor interacts with all the electrons of the valence band. Solving such a system would be impossible. However, as shown in [9], we can treat this interaction as an interaction between this given electron and the corresponding hole, with a direct term and an exchange one. As classically expected from an electric interaction between two opposite charges, the direct Coulomb interaction is attractive and therefore lower the overall energy of the system. An electron in the conduction band of a semiconductor interacts with all the electrons of the valence band. Solving such a system would be impossible. However, as shown in

[9], we can treat this interaction as an interaction between this given electron and the corresponding hole, with a direct term and an exchange one. As classically expected from an electric interaction between two opposite charges, the direct Coulomb interaction is attractive and therefore lower the overall energy of the system. An electron in the conduction band of a semiconductor interacts with all the electrons of the valence band. Solving such a system would be impossible. However, as shown in [9], we can treat this interaction as an interaction between this given electron and the corresponding hole, with a direct term and an exchange one. As classically expected from an electric interaction between two opposite charges, the direct Coulomb interaction is attractive and therefore lower the overall energy of the system.

Taking into account the symmetry of the crystal, Bir and Pikus demonstrated that the complete hamiltonian can be decomposed in two different components:
For an electron and a hole in the same Brillouin zone, the short-range exchange interaction is to be considered. It can be written:

$$\mathcal{H}_{eh}^{sr} = I_{eh}^{sr}\boldsymbol{\sigma}.\mathbf{j} + \sum_{i=x,y,z} b_i^{exch}\sigma_i j_i^3 \tag{I.49}$$

The first term lift the degeneracy between exciton of total angular moment $X = 2$ and $X = 1$. The second one take into account the reduction of symmetry in a cubic lattice and gives the dark states a fine structure. This have never been observed experimentally in bulk semiconductor, but it is expected to be much smaller than the lift induced by I_{eh}^{sr}.
For carriers in different Brillouin-zone, the long-range exchange interaction have to be considered. It mixes the bright exciton states in an anisotropic potential, such as the one of a partially relaxed self assembled quantum dot. In the heavy hole exciton subspace ($X_z = |+2\rangle, |+1\rangle, |-1\rangle, |-2\rangle$), it can be written as:

$$\mathcal{H}_{eh}^{lr} = \begin{pmatrix} 0 & 0 & 0 & 0 \\ 0 & 0 & \frac{1}{2}\delta_2 \exp(-2i\phi_2) & 0 \\ 0 & \frac{1}{2}\delta_2 \exp(-2i\phi_2) & 0 & 0 \\ 0 & 0 & 0 & 0 \end{pmatrix} \tag{I.50}$$

with δ_2 the splitting of the bright exciton induced by the exchange interaction.

In a quantum dot, the confinement of the carrier leads to a better overlap of the wave function and thus greater exchange energies. The exchange interaction has to be taken into account in order to fully understand the optical properties of such dots. Writing $\mathbf{j} = (j_z, j_+, j_-)$ and $\boldsymbol{\sigma} = (\sigma_z, \sigma_+, \sigma_-)$, we can develop the

exchange hamiltonian in a QD symmetry for a quantization axis along z:

$$\begin{aligned}\mathcal{H}_{e-h}^{exch,QD} &= 2\delta_0 J_z\sigma_z &+\frac{\delta_1}{2}\left(\exp(2i\varphi_1)j_+\sigma_- - \exp(-2i\varphi_1)j_-\sigma_+\right)\\ &&+\frac{\delta_2}{2}\left(\exp(2i\varphi_1)j_+\sigma_+ + \exp(-2i\varphi_1)j_-\sigma_-\right)\end{aligned} \tag{I.51}$$

with δ_0 representing the splitting between dark and bright exciton, δ_1 the splitting between the bright exciton states and δ_2 the splitting between the dark exciton states. δ_0 value is controlled both by long-range and short-range interaction, and is typically of about 1 meV in CdTe/ZnTe. δ_1 only appear in anisotropic quantum dot and is induced by the long-range interaction, warying between a few tens and a few hundreds of μeV. Finally, δ_2 primarily arise from the short-range interaction.

We note φ_1 the direction of the strain anisotropy in the QD. Calculating the eigenstate of the hamiltonian I.54, we find the optically active states are linearly polarized along φ_1 and $\varphi_1 + 90°$ as followed:

$$|\pi_{\varphi_1}\rangle = \frac{1}{\sqrt{2}}\left(\exp(-i\varphi_1)|+1\rangle + \exp(i\varphi_1)|-1\rangle\right) \tag{I.52}$$

$$|\pi_{\varphi_1+90°}\rangle = \frac{1}{\sqrt{2}}\left(\exp(-i\varphi_1)|+1\rangle - \exp(i\varphi_1)|-1\rangle\right) \tag{I.53}$$

This model works well for quantum dots with an elongated lens shape, in the C_{2v} symmetry. However, more realistic self-assembled quantum dots have symmetries which can deviate quite substantially from the idealized shapes of circular or ellipsoidal lenses. For a C_s symmetry (truncated ellipsoidal lens), additional terms coupling the dark and the bright excitons have to be included in the electron-hole exchange Hamiltonian. Following Ref. [10], the general form of the electron-hole exchange Hamiltonian in the heavy-hole exciton basis for a low symmetry quantum dot (C_s) is

$$\mathcal{H}_{eh} = \frac{1}{2}\begin{pmatrix} \delta_0 & e^{-i\pi/4}\delta_{11} & e^{i\pi/4}\delta_{12} & \delta_2 \\ e^{i\pi/4}\delta_{11} & -\delta_0 & e^{-i\pi/2}\delta_1 & -e^{i\pi/4}\delta_{12} \\ e^{-i\pi/4}\delta_{12} & e^{i\pi/2}\delta_1 & -\delta_0 & -e^{-i\pi/4}\delta_{11} \\ \delta_2 & -e^{-i\pi/4}\delta_{12} & -e^{i\pi/4}\delta_{11} & \delta_0 \end{pmatrix} \tag{I.54}$$

I.1.5 Valence band mixing

The long range exchange interaction split the neutral exciton bright states in two linearly polarized lines, with a 90° angle between them. However, this simple picture doesn't fit well with the data, such as presented in Fig. I.4. For once, it is clear for the neutral species (X, X^2) that the angle between the polarization of the two lines is different from 90°. Moreover, the charged species (X^+, X^-) are

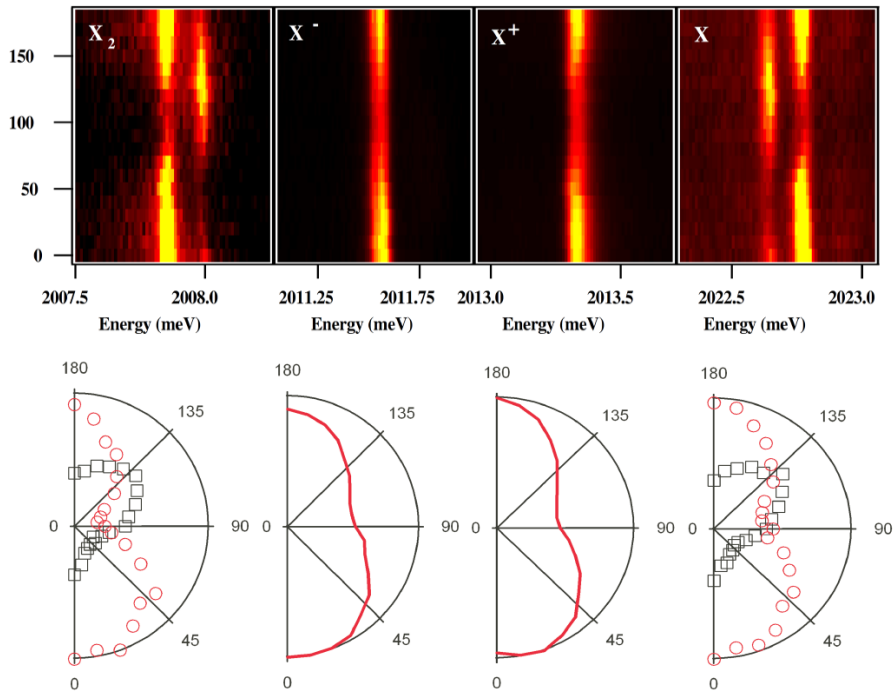

Figure I.4: PL intensities of the lines of the bi-exciton, the charged excitons and the neurtral exciton of CdTe/ZnTe quantum dot as the function of the angle of the linearly polarized detection. To simplify the reading, the intensities were also plotted on polar graph (bottom). Picture taken from Yoan Léger PhD thesis [11].

found to present linear polarization dependency, when the presence of the second hole (X^+) or electron (X^-) with an opposite spin should compensate the exciton exchange interaction, and thus these system should not present any dependency in linear polarization.

In order to fully understand it dependency, we have to stop neglecting the light hole contribution. Looking at the general form of the Luttinger hamiltonian I.13, we see that it mixes heavy hole and light hole through its non-diagonal term b_{Lutt} and c_{Lutt}. The Bir-Pikus hamiltonian I.19 presents the same symmetry and the same form as the Luttinger hamiltonian and thus also induces a coupling between the lh states and the hh states. In general, we can write the hamiltonian describing the influence of shape and strain on the valence structure in the $(|\frac{3}{2},+\frac{3}{2}\rangle, |\frac{3}{2},+\frac{1}{2}\rangle,$

$|\frac{3}{2},-\frac{1}{2}\rangle$, $|\frac{3}{2},-\frac{3}{2}\rangle$) basis as:

$$\mathcal{H}_{VBM} = \begin{pmatrix} 0 & -Q & R & 0 \\ -Q^* & \Delta_{lh} & 0 & R \\ R^* & 0 & \Delta_{lh} & Q \\ 0 & R^* & Q^* & 0 \end{pmatrix} \tag{I.55}$$

where $R = \delta_{xx,yy} - i\delta_{xy}$ describes the mixing induced by an anisotropy in the QD xy plane, $Q = \delta_{xz} - i\delta_{yz}$ stands for an asymmetry in the plane containing the QD growth axis z, and Δ_{lh} is the splitting between lh and hh induced by the in-plane bi-axial strain and the confinement. The asymmetry described by Q may come from the QD shape or the strain distribution. This hh/lh mixing is called Valence Band Mixing (VBM).

Supposing a VBM only caused by strain anisotropy, through the Bir-Pikus hamiltonian, we can write the parameters as function of the Bir-Pikus parameters and the crystal deformation ε_{ij} $(i, j = x, y, z)$ with x the (100) axis of the crystal lattice and z as defined above. The VBM parameters then writes as follow [12]:

$$\Delta_{lh} = 2b_{BP}\left(\frac{\varepsilon_{xx} + \varepsilon_{yy}}{2} - \varepsilon_{zz}\right) \tag{I.56}$$

$$R = id_{BP}\varepsilon_{xy} - b_{BP}\frac{\sqrt{3}}{2}(\varepsilon_{xx} - \varepsilon_{yy}) \tag{I.57}$$

$$Q = -\frac{2d_{BP}}{\sqrt{2}}(\varepsilon_{zx} - i\varepsilon_{zy}) \tag{I.58}$$

If we now suppose a system with pure in-plane strain anisotropy ($Q = 0$), for an origin of the energy at the top of the valence band, i.e. the hh band, we can rewrite the VBM hamiltonian in the same basis as above as:

$$\mathcal{H}_{VBM}^{in\ plane} = \begin{pmatrix} 0 & 0 & \rho_s \exp(-2i\theta_s) & 0 \\ 0 & \Delta_{lh} & 0 & \rho_s \exp(-2i\theta_s) \\ \rho_s \exp(2i\theta_s) & 0 & \Delta_{lh} & 0 \\ 0 & \rho_s \exp(2i\theta_s) & 0 & 0 \end{pmatrix} \tag{I.59}$$

with ρ_s the strain coupling amplitude and θ_s the angle between axis of the strain induced anisotropy in the QD plane and the x axis. One can notice that in the case of pure in-plane anisotropy, $|+\frac{3}{2}\rangle$ only mixes with $|-\frac{1}{2}\rangle$ and $|-\frac{3}{2}\rangle$ with $|+\frac{1}{2}\rangle$. An anisotropy along the z axis, growth axis of the dots, is needed to mix $|\pm\frac{3}{2}\rangle$ with $|\mp\frac{1}{2}\rangle$. With this notation, in the limit of weak VBM, we can now

rewrite the ground state of the holes as pseudo-spin in order to take the hh/lh mixing into account:

$$|\tilde{\Uparrow}\rangle \propto |+\frac{3}{2}\rangle - \frac{\rho_s}{\Delta_{lh}}\exp(2i\theta_s)|-\frac{1}{2}\rangle \tag{I.60}$$

$$|\tilde{\Downarrow}\rangle \propto |-\frac{3}{2}\rangle - \frac{\rho_s}{\Delta_{lh}}\exp(-2i\theta_s)|+\frac{1}{2}\rangle \tag{I.61}$$

And we have to define new angular momentum operator for these pseudo-spin:

$$\tilde{J}_+ = \frac{\rho_s}{\Delta_{lh}}\begin{pmatrix} 0 & -2\sqrt{3}\exp(-2i\theta_s) \\ 0 & 0 \end{pmatrix} \tag{I.62}$$

$$\tilde{J}_- = \frac{\rho_s}{\Delta_{lh}}\begin{pmatrix} 0 & 0 \\ -2\sqrt{3}\exp(2i\theta_s) & 0 \end{pmatrix} \tag{I.63}$$

$$\tilde{J}_s = \begin{pmatrix} \frac{3}{2} & 0 \\ 0 & -\frac{3}{2} \end{pmatrix} \tag{I.64}$$

$\tilde{J}_\pm$ are the ladder operators, flipping the hole spin, whereas $\tilde{J}_z$ return the spin value. This last operator confirm these states are mainly hh. This pseudo spin description is enough in most of the case to understand the effect of the VBM, and we will use it to study how it modify the emission of the quantum dot.

In order to do so, we begin to consider the emission of an charged state. Since, as explained earlier, the exchange interaction is null is such systems, it will allows us to focus only on the VBM effect. We can ignore the envelop function, testing mainly the overlap of the carriers wave function and thus not affecting the polarization of the emission. We write the polarization of the detection $\mathbf{e} = \cos(\alpha)\mathbf{e_x} + \sin(\alpha)\mathbf{e_y}$. We then can find the oscillator strength of the transition:

$$\begin{aligned} \Omega(\alpha) &\propto |\langle\uparrow|\cos(\alpha)p_X + \sin(\alpha)o_Y|\uparrow\downarrow\tilde{\Uparrow}\rangle|^2 \\ &= 1 + \frac{1}{3}\frac{\rho_s}{\Delta_{lh}}^2 + \frac{2}{\sqrt{3}}\frac{\rho_s}{\Delta_{lh}}\cos(2(\theta_s - \alpha)) \end{aligned} \tag{I.65}$$

with $\mathbf{p} = -i\hbar\boldsymbol{\nabla}$. Contrary to what is expected in the hh approximation, we see that the charged exciton can have a strong linear component, depending on the strength of the lh/hh mixing.

In the QD presented in Fig. I.4, the linear polarization rate $\rho_l = \dfrac{2A}{1+A^2} \approx 40\%$, with $A = \frac{\rho_s}{\sqrt{3}\Delta_{lh}}$ corresponding to a very strong lh-hh mixing, with $\frac{\rho_s}{\Delta_{lh}} \approx 0.75$. Experimentally, no correlation were found between the polarization axis of different QDs, even if they are close to each other, neither with the crystallographic axis. Such a behaviour can be explained considering the anisotropic relaxation of strains

occurring during the growth of our QDs [13]. This behaviour was also observed in III-V compounds at low QD density (near the 2D-3D transition), also attributed to the effect of strains [14]. For the III-V system, this hypothesis is supported by AFM studies showing that, in such growth conditions, the dots are preferentially nucleating near structural defects [15]. In the case of II-VI materials, a strained induced hh/lh mixing us not surprising as the dislocation formation energy is lower [16].

For the charged states X^+ and X^-, only the VBM lead to this linear polarization, leading to the simple picture discussed in this section. However, in X and X^2, the VBM and the long range exchange interaction are in competition for the polarization of the emission. The strains tend to polarized it along θ_s and $\theta_s + 90°$, when the long range exchange interaction favour linear emission along φ_1 and $\varphi_1 + 90°$. This explains that the angle between the two linearly polarized exciton lines is not equal to 90°. Moreover, the valence band mixing results in a fine structure splitting through the short range exchange interaction that can either enhance or decrease the fine structure splitting due to the long range exchange interaction. In order to illustrate our point, we consider only the isotropic part of the short range exchange interaction between the electron and the light or heavy hole:

$$\mathcal{H}_{eh}^{sr,iso} = I_{eh}\boldsymbol{\sigma}.\mathbf{J} \tag{I.66}$$

where $\frac{3}{2}I_{eh}$ corresponds to the energy splitting between bright and dark excitons due to the short range exchange interaction. The coupling between the bright states $|\downarrow \tilde{\Uparrow}\rangle$ and $|\uparrow \tilde{\Downarrow}\rangle$ through $\mathcal{H}_{eh}^{sr,iso}$ can be calculated using the pseudo-spin ladder operator defined in I.62 and I.63:

$$\langle\downarrow \tilde{\Uparrow}|\mathcal{H}_{eh}^{sr,iso}|\uparrow \tilde{\Downarrow}\rangle = \frac{1}{2\sqrt{3}} I_{eh} \frac{\rho_s}{\Delta_{lh}} \exp(-2i\theta_s) \tag{I.67}$$

Hence, the valence band mixing through the short range exchange interaction splits the bright states into two linearly polarized states along axis defined by the strain angle θ_s. The competition between this effect and the long range exchange interaction results in an angle between the two linearly polarized states different from 90°, as observed in the emission of CdTe/ZnTe QDs [17] and in InAs/GaAs ones [18]. Dark states are also coupled to each other in second order, giving them a weak oscillator strenght, with a dipole along z. A more in depth investigation of these effects was done in Yoan Léger PhD thesis [11].

I.2 Exchange interaction between carrier and magnetic atom

I.2.1 Exchange interaction in Diluted Magnetic Semiconductors

We looked until now at the structure of a so-called perfect semiconductor, without defect or impurity. However, we are interested in thesis to introduce a low density of either Manganese or Chromium atoms in the crystal, namely, impurities. A semiconductor doped in this fashion is called Diluted Magnetic Semiconductor (DMS). This magnetic atom will interact with the semiconductor electrons via its localized electrons on its exterior shell. For Mn and Cr, this orbital is the d orbital, so it will be the one considered in the following document. From the interactions between these electrons and the one in the conduction band of the semiconductor, new properties will arise. We will try in this chapter to write this interaction as a "Heisenberg" interaction:

$$\mathcal{H}_{Heisenberg} = I\boldsymbol{\sigma}.\mathbf{S} \tag{I.68}$$

with I the interaction constant, $\boldsymbol{\sigma}$ the electron spin and $\mathbf{S}$ the spin of the magnetic atom.

This formally simple interaction represents the Pauli exclusion principle through the interaction between two spins. Almost all the interactions in this chapter will be of this form, although presenting different physical processes, with only the interaction constant I varying from one another.

Both Cr and Mn are close in size to the Cd atoms they replace, so their insertion only induces a small perturbation in the crystal structure, meaning the semiconductor wave function will not be significantly altered by them. We can then as usual note the conduction electron wave function as $|\psi_{\mathbf{k}}\rangle|\sigma;\sigma_z\rangle \equiv |\psi_{\mathbf{k}};\sigma_z\rangle$, $|\psi_{\mathbf{k}}\rangle$ being the Bloch function of the semiconductor. On the other side, considering a magnetic atom at $\mathbf{r} = \mathbf{R_d}$, we write the spatial component of the wave function $\Phi_d(\mathbf{r} - \mathbf{R_d})$. Its total electronic spin, sum of the electron spins on its d orbital, is noted $|S;S_z\rangle$. The whole wave function of the magnetic atom is then $|\Phi_d;S_Z\rangle$.

Using Born-Oppenheimer approximation, we can write the hamiltonian for these electrons:

$$\mathcal{H}_{BO} = \sum_i \left(\frac{p_i^2}{2m_c} + V_c(\mathbf{r}_i)\right) + \frac{1}{2}\sum_{i,j}\frac{e^2}{4\pi\varepsilon_0|\mathbf{r_i} - \mathbf{r_j}|} \tag{I.69}$$

The first term is a single particle hamiltonian, taking into account the kinetic energy of the electron and the crystal potential $V_c(\mathbf{r}_i)$ felt by the electron at the

position $\mathbf{r}_i$. This potential includes the impurities' potential, meaning it will be different at the impurities positions rather than elsewhere in the semiconductor. The final term represents the Coulomb interaction between the electrons.

We can rewrite this hamiltonian using second quantification. We define the destruction (resp. creation) operator of a particle in the conduction band at the wave vector $\mathbf{k}$ and the spin σ as $a_{\mathbf{k},\sigma}$ (resp. $a^\dagger_{\mathbf{k},\sigma}$). In the same fashion, we define the destruction (resp. creation) operator of the electronic level of an impurity as $a_{d,S}$ (resp. $a^\dagger_{d,S}$). Supposing the number of electrons on the d orbital of the considered magnetic atom does not change, the hamiltonian I.69 then become:

$$\begin{aligned}\mathcal{H}_{SQ} &= \sum_{\mathbf{k},\sigma} E_{\mathbf{k}} a^\dagger_{\mathbf{k},\sigma} a_{\mathbf{k},\sigma} + \sum_S E_d a^\dagger_{d,S} a_{d,S} + \sum_{\mathbf{k},\mathbf{k}'} U_{\mathbf{k},\mathbf{k}'} a^\dagger_{\mathbf{k},\sigma} a_{\mathbf{k}',\sigma} \\ &\quad + \sum_{\mathbf{k},\sigma,S} M_{\mathbf{k}} (a^\dagger_{\mathbf{k},\sigma} a_{d,S} + a^\dagger_{d,S} a_{\mathbf{k},\sigma}) + \frac{1}{2} \sum_{i,j,k,l} V_{i,j,m,n} a^\dagger_i a^\dagger_j a_n a_m \qquad \text{(I.70)} \\ &= \mathcal{H}_0 + \mathcal{H}_d + V_d + \mathcal{H}_{hyb} + \mathcal{H}_{Coulomb}\end{aligned}$$

The constant electron number supposition is good enough for the picture we want to draw since most of the spin-driven interactions do not induce a change of this number.

$\mathcal{H}_0$ represents the energy of the unperturbed wave function of the semiconductor, with E_k the energy of an electron with the wave vector $\mathbf{k}$.

$\mathcal{H}_d$ is the same as $\mathcal{H}_0$ but for an electron of the d orbital of the considered magnetic impurity, with E_d the energy of an electron on this orbital.

V_d represents the impurities potential, allowing the semiconductor electrons to scatter on it. However, Mn and Cr does not modify strongly the crystal potential. We can then consider that the states of the semiconductor $|\psi_k\rangle$ are also solution of the full crystal potential, including impurity, and neglect this term.

$\mathcal{H}_{hyb}$, also called the Anderson hamiltonian, mixes the semiconductor states with the states of the impurities. It represents an exchange interaction between an electron of the semiconductor and one of the d orbital of an impurity. We can write the exchange constant as:

$$V_{kd} = \int \mathrm{d}\mathbf{r} \psi^*_k(\mathbf{r}) \mathcal{H}_1 \Phi_d(\mathbf{r} - \mathbf{R_d}) \qquad \text{(I.71)}$$

with $\mathcal{H}_1$ the one particle hamiltonian. This term depends on the Bloch state of both the semiconductor and the impurity, meaning it can be reduced to zero by the symmetry of such functions in some specific cases.

Let's now focus on last term, $\mathcal{H}_{Coulomb}$, representing the two particles exchange. i, j, m and n each represents a full wave function, both spatial and spin part, and can be either an electron of the semiconductor or of one of the impurities. We can

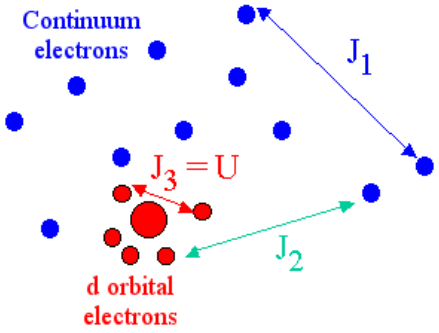

Figure I.5: Carrier interactions with no change of the number of electrons on the impurity, derived from the hamiltonian $\mathcal{H}_{Coulomb}$. Picture from Laurent Maingault PhD thesis [19].

then separate this hamiltonian in three different terms depending on the value of i, j, m and n and illustrated in Fig. I.5.

We first consider two states belonging to the continuum, appearing as J_1 on the diagram. This is the hamiltonian H_{eh} introduced in Sec. I.1.4.

The next interaction we consider is the one of two electrons from a localized atom. It represents internal transitions of the atom, representing the Hund rule. It is written:

$$\mathcal{H}_U = \sum_{d,S,S'} U a^\dagger_{d,S} a^\dagger_{d,S'} a_{d,S'} a_{d,S'} \tag{I.72}$$

with $U = \int \mathrm{d}\mathbf{r}\mathrm{d}\mathbf{r}' \dfrac{e^2}{4\pi\varepsilon_0|\mathbf{r}-\mathbf{r}'|}|\Phi_d(\mathbf{r})|^2|\Phi_d(\mathbf{r}')|^2$ the Coulomb interaction between two electrons on the same orbital with different spins. Thus, it costs more energy to add an electron on the same orbital than on another. We find back the Hund rule, with electrons first filing all orbitals with parallel spin before adding an electron to an orbital with another one, with opposed spin.

The third considered interaction is the one between an electron from the magnetic atom and an electron from the semiconductor. In the same fashion as with carriers of the bulk, it can be separated in two terms that will be developed in the next paragraphs: a direct Coulomb interaction between the two electrons, and an exchange interaction arising from the fermionic nature of electrons.

The direct Coulomb interaction doesn't depends on electrons spins. It only act on the total energy of the system and is therefore only needed when searching the

total energy of an exciton. We write it:

$$K = + \sum_{\mathbf{k},\sigma,\sigma'} K_{\mathbf{k}} a^{\dagger}_{\mathbf{k},\sigma} a^{\dagger}_{d,\sigma'} a_{d,\sigma'} a_{\mathbf{k},\sigma} \tag{I.73}$$

with

$$K_k = \int \mathrm{d}\mathbf{r}\mathrm{d}\mathbf{r}' |\psi_k(\mathbf{r})|^2 \frac{e^2}{4\pi\varepsilon_0 |\mathbf{r}' - \mathbf{r}|} |\Phi_d(\mathbf{r}')|^2$$

It is clear that the spin σ (resp. σ') of the k electron (resp. d electron) is not changed by this interaction. Since it only induce a shift in the total energy, we can redefine the origin of the energy axis to ignore it.

To go to the second term, the exchange interaction, we write it in second quantification:

$$J = + \sum_{k,k',\sigma,\sigma'} I^{ex}_{kk'} a^{\dagger}_{k',\sigma} a^{\dagger}_{d,\sigma'} a_{k,\sigma'} a_{d,\sigma} = + \sum_{k,k',\sigma,\sigma'} J_{kk'} a^{\dagger}_{k',\sigma} a_{k,\sigma'} a^{\dagger}_{d,\sigma'} a_{d,\sigma} \tag{I.74}$$

with

$$I^{ex}_{kk'} = \int \mathrm{d}\mathbf{r}\mathrm{d}\mathbf{r}' \psi^*_{k'}(\mathbf{r}) \psi^*_{k}(\mathbf{r}') \frac{e^2}{4\pi\varepsilon_0 |\mathbf{r}' - \mathbf{r}|} \Phi^*_d(\mathbf{r}) \Phi^*_d(\mathbf{r}') \tag{I.75}$$

As can be sawn on Eq. I.74, this interaction exchange the spin σ and σ' of both electrons, thus its name. Eq. I.75 shows that the spin interaction comes from a Coulomb interaction between two fermions.

We define:

$$\begin{aligned} \sigma^z_{kk'} &= a^{\dagger}_{k,\sigma} a_{k',\sigma} - a^{\dagger}_{k,-\sigma} a_{k',-\sigma} \\ \sigma^+_{kk'} &= a^{\dagger}_{k,\sigma} a_{k',-\sigma} \\ \sigma^-_{kk'} &= a^{\dagger}_{k,-\sigma} a_{k',\sigma} \end{aligned} \tag{I.76}$$

Considering now that this interaction does not change the number of electrons on the d orbital of the considered magnetic atom, we can find the Kondo hamiltonian:

$$\mathcal{H}_{sd} = - \sum_{k,k'} I^{ex}_{kk'} \boldsymbol{\sigma}_{k,k'} . \mathbf{S} \tag{I.77}$$

Since $I^{ex}_{k,k'}$ is positive, the negative sign in front of the Kondo hamiltonian shows that the energy minimum is reached when the spins of both electrons are aligned, and is therefore ferromagnetic.

We can now write the hamiltonian I.70, detailing these new hamiltonians:

$$\mathcal{H}_{SQ} = \mathcal{H}_0 + \mathcal{H}_d + \mathcal{H}_{hyb} + \mathcal{H}_{eh} + \mathcal{H}_U + \mathcal{H}_{sd} \tag{I.78}$$

with the exchange constant in $\mathcal{H}_{hyb}$, $V_{kd} = \int \mathrm{d}\mathbf{r}\psi_k^*(\mathbf{r})\mathcal{H}_1\Phi_d(\mathbf{r}-\mathbf{R_d})$.

We now have two hamiltonians to model the exchange interaction between the impurities electrons and the one in the conduction band of the semiconductor: $\mathcal{H}_{hyb}$ and $\mathcal{H}_{sd}$. Schrieffer and Wolff rewrote the Anderson hamiltonian in order to give a form closer to the Kondo hamiltonian [20]:

$$\begin{aligned}\mathcal{H}_{hyb} &= \sum_{k,k'} V_{kd}V_{k'd}\left(\frac{1}{E_k-(E_d+U)}+\frac{1}{E_{k'}-(E_d+U)}\right.\\ &\qquad\left.-\frac{1}{E_k-E_d}-\frac{1}{E_{k'}-E_d}\right)a^\dagger_{k',\sigma}a_{k,-\sigma}a^\dagger_{d,S-2\sigma}a_{d,S}\\ &= \sum_{k,k'} I^{hyb}_{kk'}a^\dagger_{k',\sigma}a_{k,-\sigma}a^\dagger_{d,S-2\sigma}a_{d,S} \qquad \text{(I.79)}\end{aligned}$$

The Fig. I.6 illustrates the different energies introduced in I.79, presenting virtual transitions to the d orbital of the magnetic atom. The two possible energies are E_d for the low energy level, and E_d+U for the high energy one, U being the energy needed to add an electron to the orbital.

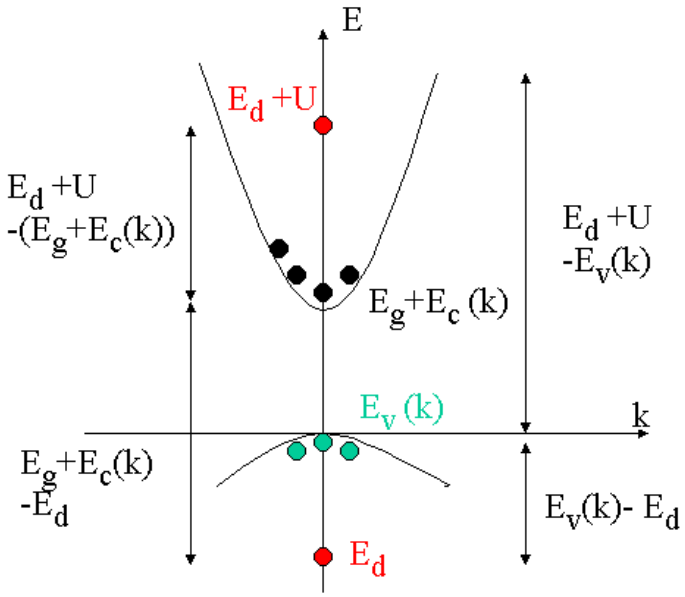

Figure I.6: Schema of the band structure and virtual transitions between valence band and conduction band. Picture from Laurent Maingault PhD thesis [19].

Doing this transformation is an important step, since we are now able to use a Heisenberg type spin hamiltonian instead of a hamiltonian mixing wave func-

tions, in addition to having the same formalism to write both type of exchange interactions, with just a difference in the exchange constants $I^{ex}_{kk'}$ and $I^{hyb}_{kk'}$.

Supposing the coupling occurs between two electrons with a close k ($k \simeq k'$), we can rewrite $I^{hyb}_{kk'}$ as:

$$\begin{aligned} I^{hyb}_{kk'} &= 2|V_{kd}|^2 \frac{U}{(E_k - E_d)(E_k - (E_d + U)} \\ &= -2|V_{kd}|^2 \frac{U}{(E_k - E_d)(E_d + U - E_k}) \end{aligned} \tag{I.80}$$

Looking ath the Fig. I.6, one can see that U and $E_k - E_d$ are both positive, while $E_k - (E_d + U)$ is negative. Thus, $I^{hyb}_{kk'}$ is negative, and we see that, while exchange leads to a ferromagnetic coupling, hybridization leads to an anti-ferromagnetic one. There will be a competition in the semiconductor between these two for every type of carrier.

Reusing the hypothesis done on Sec. I.2 of small k value, and the value of V_{kd} presented in Eq. I.71, we can rewrite the exchange constant:

$$I^{hyb}_{00,\{c,v\}} = -2 \left(\frac{U}{(E_{\{c,v\}}(0) - E_d)(E_d + U - E_{\{c,v\}}(0))} \right) \int \mathrm{d}\mathbf{r} \Phi^*_r(\mathbf{r}) \mathcal{H}_1 \psi^{\{c,v\}}_0 \tag{I.81}$$

$$I^{ex}_{00,\{c,v\}} = \int \mathrm{d}\mathbf{r}\mathrm{d}\mathbf{r}' \psi^{*\{c,v\}}_0(\mathbf{r}) \Psi^*_d \frac{e^2}{4\pi\varepsilon_0 |\mathbf{r}' - \mathbf{r}|} \psi^{\{c,v\}}_0(\mathbf{r}) \Psi_d \tag{I.82}$$

In the valence band, the semiconductor's atoms exterior orbitals have the p symmetry, as discussed in Sec. I.2. We then write I_{pd} as the sum of the hybridization and the exchange contributions:

$$I_{pd} = I^{hyb}_{00,v} + I^{ex}_{00,v} \tag{I.83}$$

In the conduction band, the orbitals are s, and so we will write the interaction I_{sd}. However, since s orbitals have a spherical symmetry, there is no hybridization contribution. The expression is then pretty easy:

$$I_{sd} = I^{ex}_{00,c} \tag{I.84}$$

Having define those, we can now rewrite the Hamiltonian of the interaction with one magnetic atom in the Heisenberg notation: Having define those, we can now rewrite the Hamiltonian of the interaction with one magnetic atom in the Heisenberg notation: Having define those, we can now rewrite the Hamiltonian of the interaction with one magnetic atom in the Heisenberg notation: Having define those, we can now rewrite the Hamiltonian of the interaction with one magnetic

atom in the Heisenberg notation: Having define those, we can now rewrite the Hamiltonian of the interaction with one magnetic atom in the Heisenberg notation:

$$\begin{aligned} \mathcal{H}_{SQ} &= \mathcal{H}_0 + \mathcal{H}_{eh} + \underbrace{I_{sd}\boldsymbol{\sigma}.\mathbf{S}} + \underbrace{I_{pd}\mathbf{J}.\mathbf{S}} \\ &= \mathcal{H}_0 + \mathcal{H}_{eh} + \quad \mathcal{H}_{sd} \quad + \quad \mathcal{H}_{pd} \end{aligned} \tag{I.85}$$

Since a DMS contain a small percentage of magnetic atoms, we can write the hamiltonian of the full semiconductor by summing on their positions. We finally get: Since a DMS contain a small percentage of magnetic atoms, we can write the hamiltonian of the full semiconductor by summing on their positions. We finally get: Since a DMS contain a small percentage of magnetic atoms, we can write the hamiltonian of the full semiconductor by summing on their positions. We finally get: Since a DMS contain a small percentage of magnetic atoms, we can write the hamiltonian of the full semiconductor by summing on their positions. We finally get: Since a DMS contain a small percentage of magnetic atoms, we can write the hamiltonian of the full semiconductor by summing on their positions. We finally get: Since a DMS contain a small percentage of magnetic atoms, we can write the hamiltonian of the full semiconductor by summing on their positions. We finally get: Since a DMS contain a small percentage of magnetic atoms, we can write the hamiltonian of the full semiconductor by summing on their positions. We finally get: Since a DMS contain a small percentage of magnetic atoms, we can write the hamiltonian of the full semiconductor by summing on their positions. We finally get:

$$\mathcal{H}_{DMS} = \mathcal{H}_0 + \mathcal{H}_{eh} + \sum_i I_{sd}(\mathbf{R}_i)\boldsymbol{\sigma}.\mathbf{S}_i + \sum_i I_{pd}(\mathbf{R}_i)\mathbf{J}.\mathbf{S}_i \tag{I.86}$$

This can be further simplified with two approximations. First, since conduction electron sees a lot of different atomic sites, we can we can work with the mean value of the magnetic atoms spins, $\langle\mathbf{S}\rangle$, instead of their individual value $\mathbf{S}_i$. This is the mean field approximation, the magnetic atoms being seen as an effective magnetic field. And for the same reason, we can consider the electron interaction with each site of the crystal multiplied by the probability x of being occupied by a magnetic atom, instead of summing only on the magnetic atoms positions. This is the virtual crystal approximation. We can then rewrite:

$$\sum_i I_{sd}(\mathbf{R}_i)\boldsymbol{\sigma}.\mathbf{S}_i = x\sum_{\mathbf{R}} I_{sd}(\mathbf{R})\boldsymbol{\sigma}.\langle\mathbf{S}\rangle \tag{I.87}$$

Projecting along the quantization axis, we just replace $\boldsymbol{\sigma}.\langle\mathbf{S}\rangle$ by $\sigma_z\langle S_z\rangle$. Since the atoms are seen as a magnetic field, they induce a degeneracy lift ΔE_c between the two spin values of conduction electron, $|\sigma_z = \pm\frac{1}{2}\rangle$:

$$\Delta E_c = N_0 x\alpha\sigma_z\langle S_z\rangle \tag{I.88}$$

with $\alpha \propto I_{sd}^{00}$ the interaction constant between the impurity's and the conduction band's Bloch function at $\mathbf{k} = 0$, and N_0 the number of cell per volume.

The same consideration can be done for valence band. Hh and lh are separated via their spin values: $|J_z = \pm\frac{3}{2}\rangle$ for hh, $|J_z = \pm\frac{1}{2}\rangle$ for lh. We then get:

$$\Delta E_v = N_0 x \frac{\beta}{3} J_z \langle S_z \rangle \tag{I.89}$$

with $\beta \propto I_{pd}^{00}$ the impurity's and the valence band's Bloch function at $\mathbf{k} = 0$.

To be completely thorough with the analysis, we should also take into account the confinement due to the quantum dot. This means the wave vector $\mathbf{k}$ of the carriers can be different from 0, leading to small perturbative effect on $\mathcal{H}_{sd}$ and $\mathcal{H}_{pd}$. This was done thoroughly by Laurent Maingault in the Chap. I.3 of his PhD thesis [19]. It is shown that the hamiltonian changed as follow:

$$\begin{aligned}\mathcal{H}_{sd}(\mathbf{R}) = -\alpha \boldsymbol{\sigma}.\mathbf{S} \left| F_c(\mathbf{R}) - A_2 \left(\frac{\partial^2 F_c}{\partial z^2}(\mathbf{R}) + \frac{\partial^2 F_c}{\partial \rho^2}(\mathbf{R}) \right) \right|^2 \\ - \beta \boldsymbol{\sigma}.\mathbf{S} \left((C_2 - B_2) \left| \frac{\partial^2 F_c}{\partial z^2}(\mathbf{R}) \right|^2 + C_2 \left| \frac{\partial^2 F_c}{\partial \rho^2}(\mathbf{R}) \right|^2 \right)\end{aligned} \tag{I.90}$$

$$\mathcal{H}_{pd}(\mathbf{R}) = -\beta \mathbf{J}.\mathbf{S} |F_v(\mathbf{R}) - V_{kd} F_v''(\mathbf{R})|^2 \tag{I.91}$$

with $F_c(\mathbf{R})$ (resp. $F_v(\mathbf{R})$) the electron (resp. hole) envelop function, $F_v''(\mathbf{R})$ the second derivative of the hole envelop function, and A_2, B_2, C_2 constant depending on the semiconductor lattice. For CdTe, $A_2 = 10.3$ Å^{-2}, $B_2 = 0.781$ Å^{-2} and $C_2 = 19.8$ Å^{-2}.

I.2.2 Studied magnetic atoms: Mn and Cr

We will consider in the section the interaction between single magnetic atoms trapped in quantum dots and the carrier. Specifically, we will be interested in the interaction with a Manganese atom and with a Chromium atom. This does not change dramatically the picture we draw in the previous section. However, for the interaction between the semiconductor electrons and the magnetic atom d electrons, we will have to also take into account the overlap between the magnetic atom and the carriers. For a magnetic atom A, we then defined the exchange constant:

$$I_{eA} = \alpha |F_c(\mathbf{R})|^2 \tag{I.92}$$

$$I_{hA} = \beta |F_v(\mathbf{R})|^2 \tag{I.93}$$

Mn in CdTe

Using the exchange constant defined above, we can rewrite the hamiltonian I.85:

$$\begin{aligned} \mathcal{H}_{cMn} &= \mathcal{H}_{eMn} + \mathcal{H}_{hMn} \\ &= I_{eMn}\boldsymbol{\sigma}.\mathbf{S}_{Mn} + I_{hMn}\mathbf{J}.\mathbf{S}_{Mn} \end{aligned} \tag{I.94}$$

We ignore $\mathcal{H}_0$ here since it only shift the energy of the system without affecting the spins exchange interactions. In II-VI semiconductors, Mn is inserted as Mn^{2+}, with an electronic spin $S = \frac{5}{2}$. We can then write its spin operator as we did for the carrier in Sec. I.2:

$$S_{Mn,x} = \begin{pmatrix} 0 & \frac{\sqrt{5}}{2} & 0 & 0 & 0 & 0 \\ \frac{\sqrt{5}}{2} & 0 & \sqrt{2} & 0 & 0 & 0 \\ 0 & \sqrt{2} & 0 & \frac{3}{2} & 0 & 0 \\ 0 & 0 & \frac{3}{2} & 0 & \sqrt{2} & 0 \\ 0 & 0 & 0 & \sqrt{2} & 0 & \frac{\sqrt{5}}{2} \\ 0 & 0 & 0 & 0 & \frac{\sqrt{5}}{2} & 0 \end{pmatrix}$$

$$S_{Mn,y} = \begin{pmatrix} 0 & -\frac{i\sqrt{5}}{2} & 0 & 0 & 0 & 0 \\ \frac{\sqrt{5}}{2} & 0 & -i\sqrt{2} & 0 & 0 & 0 \\ 0 & \sqrt{2} & 0 & -\frac{3i}{2} & 0 & 0 \\ 0 & 0 & \frac{3}{2} & 0 & -i\sqrt{2} & 0 \\ 0 & 0 & 0 & \sqrt{2} & 0 & -\frac{i\sqrt{5}}{2} \\ 0 & 0 & 0 & 0 & \frac{\sqrt{5}}{2} & 0 \end{pmatrix} \tag{I.95}$$

$$S_{Mn,z} = \begin{pmatrix} \frac{5}{2} & 0 & 0 & 0 & 0 & 0 \\ 0 & \frac{3}{2} & 0 & 0 & 0 & 0 \\ 0 & 0 & \frac{1}{2} & 0 & 0 & 0 \\ 0 & 0 & 0 & -\frac{1}{2} & 0 & 0 \\ 0 & 0 & 0 & 0 & -\frac{3}{2} & 0 \\ 0 & 0 & 0 & 0 & 0 & -\frac{5}{2} \end{pmatrix}$$

In the conduction band, the electrons s orbitals are orthogonal to the d orbital of the Mn atom. No hybridization can then occur between these. Only the Coulomd interaction remain, leading to an overall ferromagnetic interaction between conduction band electrons and Mn electronic spin. Confirming this, $N_0\alpha = 0.22 \pm 0.01$ eV was measured [21].

The deduction is a bit harder to work out in the valence band. Valence electrons p orbitals are not orthogonal to Mn electrons d orbital, meaning there is a competition between the ferromagnetic Coulomb interaction and the anti-ferromagnetic

hybridization. However, the hybridization is usually stronger than Coulomb interaction for Mn in II-VI semiconductor, leading to an overall anti-ferromagnetic interaction between holes and Mn electronic spin [22]. For $Cd_xMn_{1-x}Te$, $N_0\beta = -0.88 \pm 0.01$ eV was measured, confirming this tendency [21].

Cr in CdTe

As for the Mn, we can rewrite the hamiltonian I.85 using the exchange interaction defined in the introduction of this section:

$$\begin{array}{rcccc} \mathcal{H}_{cCr} & = & \mathcal{H}_{eCr} & + & \mathcal{H}_{hCr} \\ & = & I_{eCr}\boldsymbol{\sigma}.\mathbf{S}_{Cr} & + & I_{hCr}\mathbf{J}.\mathbf{S}_{Cr} \end{array} \tag{I.96}$$

Once again, we ignore $\mathcal{H}_0$ since it didn't affect the spins exchange interaction. We can also write the Cr spin operators as follow:

$$\begin{aligned} S_{Cr,x} &= \begin{pmatrix} 0 & 1 & 0 & 0 & 0 \\ 1 & 0 & \sqrt{\frac{3}{2}} & 0 & 0 \\ 0 & \sqrt{\frac{3}{2}} & 0 & \sqrt{\frac{3}{2}} & 0 \\ 0 & 0 & \sqrt{\frac{3}{2}} & 0 & 1 \\ 0 & 0 & 0 & 1 & 0 \end{pmatrix} \\ S_{Cr,y} &= i \begin{pmatrix} 0 & -1 & 0 & 0 & 0 \\ 1 & 0 & -\sqrt{\frac{3}{2}} & 0 & 0 \\ 0 & \sqrt{\frac{3}{2}} & 0 & -\sqrt{\frac{3}{2}} & 0 \\ 0 & 0 & \sqrt{\frac{3}{2}} & 0 & -1 \\ 0 & 0 & 0 & 1 & 0 \end{pmatrix} \\ S_{Cr,z} &= \begin{pmatrix} 2 & 0 & 0 & 0 & 0 \\ 0 & 1 & 0 & 0 & 0 \\ 0 & 0 & 0 & 0 & 0 \\ 0 & 0 & 0 & -1 & 0 \\ 0 & 0 & 0 & 0 & -2 \end{pmatrix} \end{aligned} \tag{I.97}$$

For conduction band electrons, the situation is the same as with the Mn: the conduction electrons s orbital are orthogonal to the Chromium d orbital, and the hybridization is then null. Hence, only the Coulomb interaction remain and induce a ferromagnetic coupling between the electrons of the band and the Cr electronic spin. $N_0\alpha$ was never measured in $Cd_xCr_{1-x}Te$, but most most magnetic atoms

in II-VI semiconductor presents a value between 0.2 eV and 0.3 eV. It is then generally assume that, in II-VI semiconductor, $N_0\alpha \approx 0.2$ eV [23].

Once again, valence band is a bit more complicated: Coulomb interaction, leading a ferromagnetic coupling, competes with hybridization between valence band p electrons and Cr d electrons. Direct measure of $N_0\beta$ was neither done in $Cd_xCr_{1-x}Te$, so the competition between these two interactions is difficult to evaluate. Moreover, it has been showed that it was difficult to decide theoretically if the interaction between Cr and holes was ferromagnetic or anti-ferromagnetic both in CdTe and in ZnTe [24]. However, it was found that $N_0\beta$ was positive in $Cd_xCr_{1-x}S$ [25] and in most Zn based II-VI semiconductors, assuming $N_0\alpha = 0.2$ eV [22]. Especially, in ZnTe, still using this assumption, $N_0\beta = +3.6 \pm 1.2$ eV was found [23]. Since there is almost no valence band offset between ZnTe and CdTe, it seems safe to assume that $N_0\beta$ in CdTe is positive and thus the interaction between Cr and holes is ferromagnetic.

I.3 Fine and hyperfine structure of a magnetic atom in II-VI semiconductor

I.3.1 Mn atom in II-VI semiconductor

Mn is incorporated in II-VI semiconductors as Mn^{2+}. This ion is really weakly coupled to the strain state at its position. In first approximation, we can then consider it as an isolated ion occupying a cation site in the lattice. We will first study the free ion and then see the effect of the lattice on the different states.

The Mn^{2+} electronic structure $[Ar]3d^5$. Since the d orbital is five time degenerated (doubled when taking spin into account), it is half-full in the case of the Mn in II-VI. Following Hund's rule, the spin of those electron are all aligned, leading to an electron spin $S = \frac{5}{2}$ and, following Pauli exclusion principle ranging the electrons angular momenta from -2 to $+2$, an angular momentum $L = 0$.

We get from Hund's rule that adding an electron to an half-full orbital has a high energy cost. The lowest energy excited states are therefore the flipping of an electron. For a free atom, it leads to a first excited state with an angular moment $L = 4$. Following the spectroscopic notation of these states ${}^{(2S+1)}L$, the ground state is the noted ${}^6S$ ($L = 0$, $S = \frac{5}{2}$) and the first excited state is ${}^4G$ ($L = 4$, $S = \frac{3}{2}$). The flipping of one electron leads also to higher energy excited states, written in spectroscopic notation ${}^4P$, ${}^4D$ and ${}^4F$ in Fig. I.7.

Mn atom in inserted in the CdTe lattice replacing a Cd atom. The interaction with the crystal field will lift the degeneracies of the free atom level. Those new levels are written with the appropriate group theoritical transformation properties. The ${}^6S$ ground state is symmetrical and non-degenrated. Thus, in first order, it

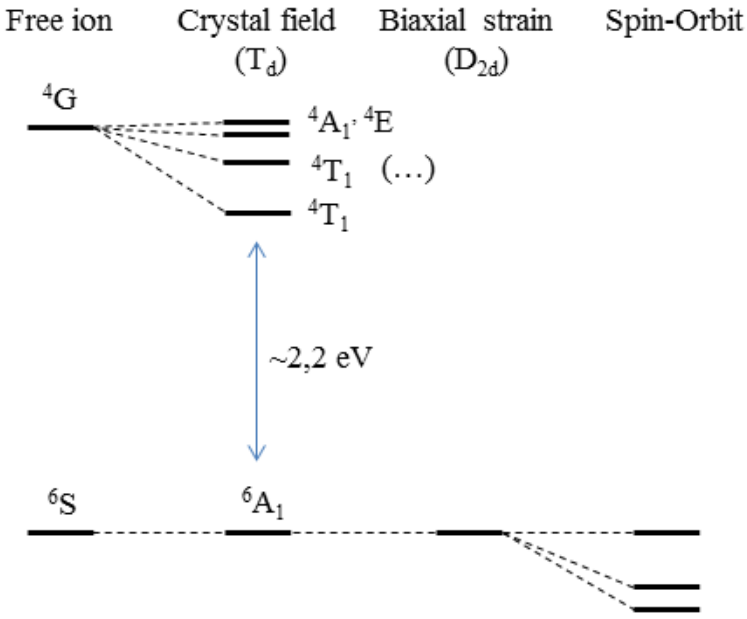

Figure I.7: A schematic diagram of the splitting of the lowest excited states of the $3d^5$ level (^{4}G) relative to the ground state (^{6}S) for a Mn^{2+} ion in the presence of a tetrahedral crystal field.

is not affected by the crystal field and is noted $^6A_1$. On the other hand, ^{4}G, the first excited state, is degenerated and therefore is affected by the crystal. It split into four different states: $^4T_1$, three-fold degenerated ; $^4T_2$, three-fold degenerated ; ^{4}E, two-fold degenerated ; and $^4A_1$, not degenerated. It has been shown by calculations that the effect of the crystal field is to pull the two ^{4}T levels closer to the ground state, while ^{4}E and $^4A_1$ are almost coincident and almost not affected by the crystal field [26–28]. Higher energy excited states would also be affected, but they are at high enough energy for their contribution not to be significant.

For a free atom, the transition between the ground state with $S = \frac{5}{2}$ and any of the excited state, with $S = \frac{3}{2}$ is forbidden by the $\Delta S = 0$ rule and the parity selection ones. However, in a II-VI lattice, the spin-orbit interaction and the absence of inversion symmetry relax those rules, and thus allow the transitions between $^6A_1$ and the different states coming from the ^{4}G splitting. $^6A_1 \rightarrow ^4T_1$ is the lowest energy of those transitions and therefore the most significant. It corresponds to approximately 2.2 eV. We saw in Sec. I.2 that CdTe band gap was 1.6 eV at 5K, far from the Mn internal transition energy. The confinement, however, will increase the energy of the carriers in the quantum dot, getting them closer to the internal transition. To keep a strong enough luminescence, we then have to be wary of the size of our studied dots in order to stay far enough from

these Mn transitions.

^{6}A state of the Mn^{2+} is symmetric and thus almost not affected by the crystal field. However weakly, Mn^{2+} is still sensible to strain state at its position, leading to the Mn^{2+} strain induced fine structure. We can, in the equation, also take into account the hyperfine structure induced by the nuclear spin $I = \frac{5}{2}$ of the Mn atom. The Hamiltonian of the coupled electronic an nuclear spins of a Mn atom in a strained layer grow along [001] axis is known from electron paramagnetic resonance in CdTe/ZnTe superlattices [29] and reads:

$$\begin{aligned} \mathcal{H}_{Mn} &= \mathcal{A}\mathbf{I}.\mathbf{S} \\ &+\frac{1}{6}a(S_x^4+S_y^4+S_z^4-\frac{1}{5}S(S+1)(3S^2+3S-1)) \\ &+D_0(S_z^2-\frac{1}{3}S(S+1))+E(S_y^2-S_x^2) \end{aligned} \tag{I.98}$$

The first term is the hyperfine interaction between the Mn nuclear spin $\mathbf{I}$ and its $5d$ electrons spin $\mathbf{S}$, coupling two consecutive Mn spin states through an electron-nuclei flip flop. The hyperfine constant of the Mn was found to be $\mathcal{A} \approx 0.71$ μeV [30]. The second term results from the crystal cubic symmetry and mixes different S_z of the Mn spin. According to ref. [30], we have $a = 0.32$ μeV.

The last line contains terms linked to the strain state at the Mn position: the magnetic anisotropy caused by bi-axial strain D_0 and the anisotropy of strain in the xy plane E. D_0 is the dominant term for a Mn atom in a highly strained QD. Because of the partial relaxation of strain in the self-assembled QD we used, the value of D_0 may vary between 0 μeV for a strain-free QD, to 12 μeV for a fully strain CdTe layer matched on ZnTe. It splits the Mn spin states according to S_z^2 and is responsible for the Mn spin memory at zero magnetic field [31].

The anisotropy in the QD plane induces a mixing between different S_z through the anisotropic crystal field component E. It coupled two values of S_z separated by two units of spin. In the absence of magnetic anisotropy ($D_0 \simeq 0$), both the anisotropy of strain and the hyperfine structure prevent the optical pumping of the Mn spin at 0 magnetic field.

I.3.2 Cr atom in II-VI semiconductor

Cr atoms are incorporated into II-VI semiconductors as Cr^{2+} ions on cation sites forming a deep impurity level. This isotope presents *no nuclear spin*, meaning we don't have to consider the hyperfine structure of a Cr atom in a II-VI semiconductor. The ground state of a free Cr^{2+} is ^{5}D with the orbital quantum number $L = 2$ and a spin $S = 2$ yielding a 25-fold degeneracy. In the crystal field of T_d symmetry of the tetrahedral cation site in zinc-blende crystal, the degeneracy is partially lifted (see Fig. I.3.2): the ^{5}D term splits into 15-fold degenerate orbital

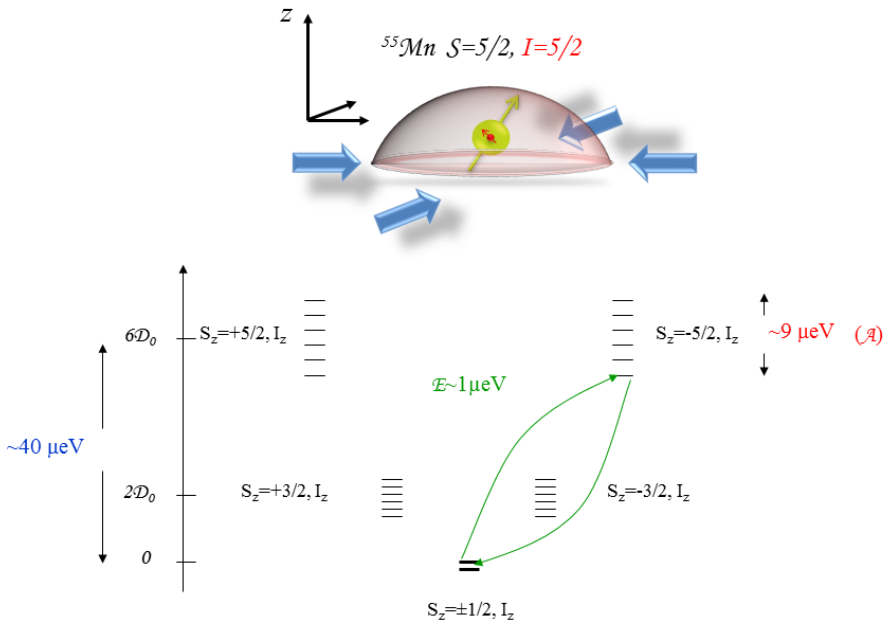

Figure I.8: Top: picture of an idealized strained QD containing a magnetic atom. Bottom: scheme of the energy level of a Mn atom in a strained II-VI QD. All the stable Mn isotopes ^{55}Mn carries a nuclear spin $I = \frac{5}{2}$ which couples through the hyperfine interaction ($\mathcal{A}\mathbf{I}.\mathbf{S}$) to the electronic spin $S = \frac{5}{2}$.The d orbital of the Mn is also sensitive to the electric field produced by the neighbouring crystal atoms (crystal field) in the zinc-blend lattice. A distortion of the lattice and consequently a change in the crystal field will also affect the d orbital. The dynamic of the Mn spin at zero magnetic field is mainly controlled by a magnetic anisotropy D_0 produced by the presence of a large bi-axial strain at the Mn location. This field splits the spin states of the Mn according to $D_0 S_z^2$; the anisotropy of the strain in the quantum dot plane ($E(S_y^2 - S_x^2)$) also mix the different S_z component (green arrow).

triplet ^{5}T$_2$ and 10-fold degenerate orbital doublet ^{5}E. The substitution of a Cd atom by a Cr atom lead to a Jahn-Teller distortion of the tetragonal matrix [32]. This distortion reduces the symmetry to D$_{2d}$ and leads to a splitting of the ^{5}T$_2$ ground state into a 5-fold degenerate ^{5}B$_2$ orbital singlet and a ^{5}E orbital doublet.

The ground state orbital singlet ^{5}B$_2$ is further split by the spin-orbit interaction. In a strain free crystal, it was found that the ground state splitting can be described

by the spin effective Hamiltonian [32]:

$$\mathcal{H}_{Cr,CF} = D_0 S_z^2 + \frac{1}{180} F[35S_z^2 - 30S(S+1)S_z^2 + 25S_z^2] + \frac{1}{6} a[S_1^4 + S_2^4 + S_3^4] \tag{I.99}$$

with the Cr spin $S = 2$ and $|D_0| \gg |a|, |F|$. In the model presented here, we use $a = 0$ and $F = 0$. The x, y, z principal axes were found to coincide with the cubic axes (1,2,3) giving rise to three identical sites, each given by I.99 but with the z axis of each along a different cubic axis (1,2,3). A value of $D_0 \approx +30$ μeV was estimated from Electron Paramagnetic Resonance (EPR) measurements in highly diluted bulk (Cd,Cr)Te [32].

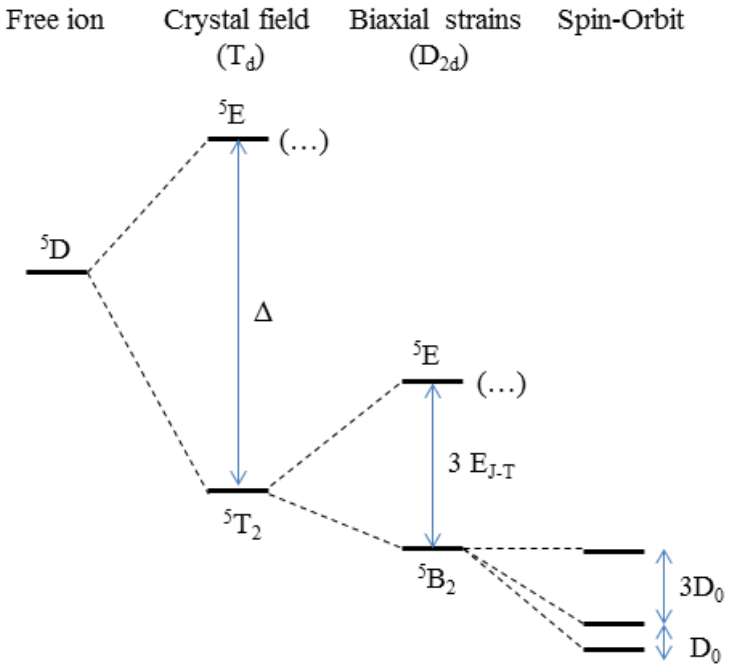

Figure I.9: Schema of the energy level splitting of Cr^{2+} at a cation site in II-VI compounds having zinc blende structure (T_d) with a crystal field parameter Δ, a Jahn-Teller energy E_{J-T} and a spin-orbit level spacing D_0.

Static biaxial compressive strain in the (001) plane, as observed in self-assembled quantum dots, reduces the symmetry to D_{2d} and destabilize the Cr $3d$ orbitals d_{xz} and d_{yz} having an electron density pointing along the [001] axis (z axis). The Cr ground state is then a 5-fold degenerated orbital singlet formed from the d_{xy} orbital. It corresponds to the Jahn-Teller ground state with a tetragonal distortion along the [001] axis [33].

An applied stress will also influence the Cr spin fine structure splitting through the modification of the crystal field and the spin-orbit interaction [32]. For an arbitrary strain tensor, the general form of the Cr ground state spin effective Hamiltonian is

$$\mathcal{H}_{Cr,\varepsilon} = c_1 e_A S_\theta + c_2 e_\theta S_\theta + c_3 e_\epsilon S_\epsilon + c_4 e_\zeta S_\zeta + c_5 (e_\xi S_\xi + e_\eta S_\eta) \tag{I.100}$$

with S_i defined as:

$$\begin{aligned} S_\theta &= S_z^2 - \frac{1}{2}[S_x^2 + S_y^2] \\ S_\epsilon &= \frac{1}{2}\sqrt{3}[S_x^2 - S_y^2] \\ S_\xi &= S_y S_z + S_z S_y \\ S_\eta &= S_x S_z + S_z S_x \\ S_\zeta &= S_x S_y + S_y S_x \end{aligned} \tag{I.101}$$

and e_i defined similarly as:

$$\begin{aligned} e_\theta &= \varepsilon_{zz} - \frac{1}{2}[\varepsilon_{xx} + \varepsilon_{yy}] \\ e_\epsilon &= \frac{1}{2}\sqrt{3}[\varepsilon_{xx} - \varepsilon_{yy}] \\ e_\xi &= \varepsilon_{yz} + \varepsilon_{zy} \\ e_\eta &= \varepsilon_{xz} + \varepsilon_{zx} \\ e_\zeta &= \varepsilon_{xy} + \varepsilon_{yx} \\ e_A &= \varepsilon_{xx} + \varepsilon_{yy} + \varepsilon_{zz} \end{aligned} \tag{I.102}$$

As shown in Sec. I.1.2, we can write for a flat self-assembled quantum dot with dominant large biaxial strain:

$$\begin{aligned} \varepsilon_{xx} &= \varepsilon_{yy} = \varepsilon_\parallel \\ \varepsilon_{zz} &= -2\frac{C_{11}}{C_{12}}\varepsilon_\parallel \end{aligned}$$

where $C_{11} \approx 5.4\ 10^{10}$ Pa and $C_{12} \approx 3.7\ 10^{10}$ Pa are the elastic constants of CdTe [34]. For this strain configuration, the Cr fine structure is controlled by the spin-lattice coupling coefficients c_1 (symmetric coefficient) and c_2 (tetragonal coefficients). Strain-coupling coefficients estimated from EPR measurements in bulk Cr doped CdTe are listed in table I.2.

We can now simplify the hamiltonian I.100, first reducing it to the active term in our case:

$$\mathcal{H}_{Cr,\varepsilon} = c_1 e_A S_\theta + c_2 e_\theta S_\theta$$

Table I.2: Values for spin to strain coupling coefficients of Cr in bulk CdTe (in meV) extracted from ref. [32].

c_1	c_2	c_3	c_4	c_5
-0.25±2	+4.9 ±2	-1.25±0.5	+4.9±2	+3.7±1.25

Replacing now e_A, e_θ and S_θ by their value given in I.101 and I.102, and using the equalities given in Sec. I.1.2, we can rewrite the strain controlled part of the spin Hamiltonian as $\mathcal{H}_{Cr,\varepsilon}$, depending only on $\varepsilon_\parallel$:

$$\begin{aligned} \mathcal{H}_{Cr,\varepsilon_\parallel} &= \underbrace{\frac{3}{2}\varepsilon_\parallel[2c_1(1-\frac{C_{12}}{C_{11}}) - c_2(1+2\frac{C_{12}}{C_{11}})]}_{D_0} \; S_z^2 \\ &= D_0 \; S_z^2 \end{aligned} \tag{I.103}$$

where we can estimate $D_0 \approx 1 \pm 0.6$ meV from the values of the spin-strain coupling coefficients in CdTe (table I.2). However one should note the quantum dots could be partially relaxed and may contain a significant amount of Zn. We were not able to find spin to strain coupling coefficients for Cr in ZnTe and (Cd,Zn)Te alloy in literature. A value of $D_0 \approx +280$ μeV, much larger than for CdTe, was however estimated in strain-free Cr-doped bulk ZnTe [32]. Larger spin-strain coupling coefficients could than expected for Cr in ZnTe and (Cd,Zn)Te alloys.

Finally, an anisotropy of the strain in the quantum dot plane (001) with principal axis along [010] or [100] axes ($\varepsilon_{xx} \neq \varepsilon_{yy}$ and $\varepsilon_{xy} = \varepsilon_{yx} = 0$) would affect the Cr fine structure through the tetragonal coefficient c_3. This coupling can be described by an additional term in the spin-strain Hamiltonian

$$\begin{aligned} \mathcal{H}_{Cr,\varepsilon_\perp} &= \underbrace{\frac{3}{4}c_3(\varepsilon_{xx} - \varepsilon_{yy})}_{E} \; (S_y^2 - S_x^2) \\ &= E \; (S_y^2 - S_x^2) \end{aligned} \tag{I.104}$$

This anisotropy term E couples Cr spin states separated by two units and in particular S_z=+1 to S_z=-1 which are initially degenerated. It could be exploited to induce a large strain mediated coherent coupling between a mechanical oscillator and the Cr spin [35].

We can now group I.103 and I.104 in order to write the complete hamiltonian of an isolated Cr in a strained, anisotropic CdTe/ZnTe quantum dot:

$$\begin{aligned} \mathcal{H}_{Cr,\varepsilon} &= \mathcal{H}_{Cr,\varepsilon_\parallel} + \mathcal{H}_{Cr,\varepsilon_\perp} \\ &= D_0 S_z^2 + E(S_y^2 - S_x^2) \end{aligned} \tag{I.105}$$

I.4 A simple example: the X-Mn system

In order to illustrate the concepts explained in this chapter, we will do a quick study of a well known system: the exciton coupled to a single Manganese atom. In order to simplify the study, let's consider a QD containing a single Mn atom with no shape or strain anisotropy. When an exciton is injected in, it will interact with the magnetic atom on top of the hole-electron interaction already taking place for an exciton. We can then write the hamiltonian of these system:

$$\mathcal{H}_{XMn} = \mathcal{H}_{eh} + \mathcal{H}_{eMn} + \mathcal{H}_{hMn} \tag{I.106}$$

We use in this part the heavy-hole approximation, ignoring the effect of the non-diagonal term of the band hamiltonian. In order to simplify the notation, we write $|S_{z,Mn}\rangle = |S_z\rangle$.

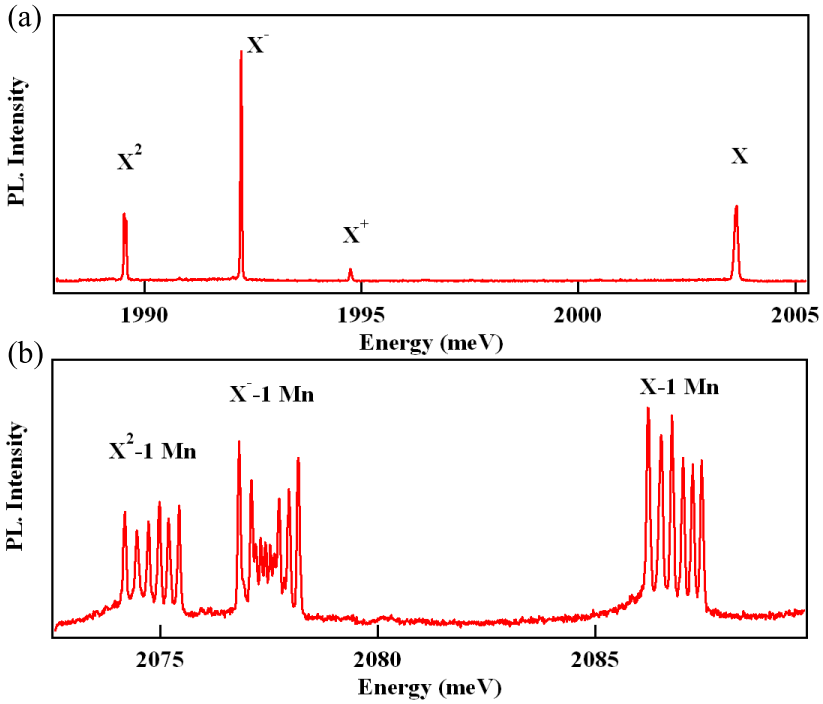

Figure I.10: Photoluminescence of the X, X^- and X^2 complex for (a) a undoped QD and (b) a QD containing a single Mn atom.

In the heavy hole subspace, in the σ_z, j_z, S_z basis, all the hamiltonians describing an interaction with the hole are diagonal. Therefore, the only non-diagonal element in the hamiltonian I.106 describe electron-Mn spin-flips. The hole having no part in this interaction, those spin-flips couple a bright state to a dark

state, separated by δ_0, as defined in Sec. I.1.4. The strength of this interaction is of the same magnitude of I_{eMn}, found to in the 100 μeV range in our quantum dots [36]. The distance between the bright and dark states is then about one order of magnitude higher than the strength of the interaction. We thus chose to ignore it.

We can then consider the hamiltonian I.106 to be diagonal. The interaction of the Mn spin with electron is ferromagnetic with $I_{eMn} \simeq -100$ μeV, while its interaction with the hole is anti-ferromagnetic with $I_{hMn} \simeq 250$ μeV. The carriers act as an effective magnetic field along the growth axis. This lift the degeneracy of the Mn spins in a sextuplet. For the bright exciton, with anti-parallel spins, the lift is the strongest. Each Mn spin state is separated from the closest one by $\frac{1}{2}(3I_{hMn} - I_{eMn})$, for a total energy span of $\frac{5}{2}(3I_{hMn} - I_{eMn})$. For the dark exciton states, each of them are separated from the closest one by $\frac{1}{2}(3I_{hMn} + I_{eMn})$, for total energy span of $\frac{5}{2}(3I_{hMn} + I_{eMn})$.

One can note that the system is symmetric under inversion of the quantification axis z. Excitons with opposed spins coupled to opposed Mn spins will then be degenerated. Example given, $|S_z = \frac{5}{2}, X_z = -1\rangle$ share the same energy level as $|S_z = -\frac{5}{2}, X_z = +1\rangle$. The whole energy level structure is summarize in Fig. I.11.

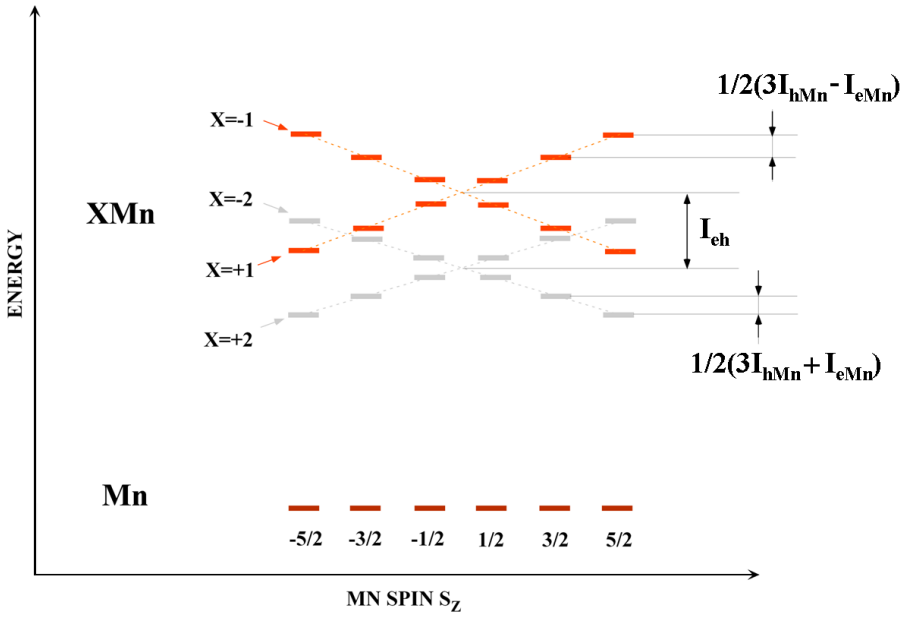

Figure I.11: Energy level of the ground state and the exciton in a Mn-doped QD. The levels are sketched as a function of the Mn spin S_z. Dark states are represented in grey. Optical transitions from the bright states of the Mn complex results in six-line PL spectra, such as in Fig. I.10.

The fundamental state of the QD is an isolated Mn atom in the dot. We found in our QDs a maximum D_0 of 12 μeV, negligible compared to the exciton-Mn interactions. Since the other fine structure parameters of the Mn are less intense than D_0, we choose to neglect their contribution to the spectra. Therefore, the fundamental state of the QD is six time degenerated. The recombination does not affect the Mn spin. Each emission line is thus the superposition of two optical transitions with opposed circular polarization (recombination of an excition $X_z = \pm 1$). In a given polarization, each line corresponds then to a single Mn spin: the spectra is a photography of the statistic state of the Mn spin during the exciton recombination.

This simple model is however incomplete: one can see on Fig. I.10 that each peak as a different intensity, which is not explained by the model described here. More thorough investigation of the system were done in [11]. The effect of the VBM on the system was studied in [17]. A complete study of the dynamic of the system was done by Claire Le Gall in her PhD thesis [3].

[capbesideposition=right,center]floatrow

Chapter II

Magneto-optical study of Cr-doped CdTe quantum dots

In this chapter, we will study the photoluminescence of a II-VI quantum dot containing a single Chromium atom. We saw in the Sec. I.3.2 that the magnetic anisotropy of the spin leads to a zero magnetic field splitting of the 0, ± 1 and ± 2 states. In a neutral Cr-doped quantum dot, such an anisotropy is induced by the bi-axial strains in the plane of the dots. Probing optically the dot, it results that exchange interaction is enough to see the effect of the presence of a single Cr spin in the QD. Studying the magnetic-field dependence of the quantum dots photoluminescence also shows the influence of the symmetry on carrier-Cr spin coupling.

The chapter is organized as follows. First, we present the photoluminescence of several dots, extracting the Cr energy structure from it. Several features of this luminescence is then discussed. The study of the dot emission under magnetic field confirm the chosen energy structure. In the second section, we explain the model in more details, extracting parameters from the magneto-optics experiment, and examining its prediction for a different type of QD. Finally, we present and give a possible explanation to dots not explained by the model presented in this chapter.

II.1 Strained quantum dots containing an individual Cr atom

II.1.1 Energy structure of a Cr in a quantum dot

Using the procedure described in the Sec. II.1, we randomly incorporated Cr atoms in CdTe/ZnTe quantum dots, adjusting the density of the Cr atoms to be roughly equal to the density of dots, in order to get QDs containing 0, 1 or a few Cr atoms.

The photoluminescence (PL) of individual QDs, induced by optical excitation with a dye laser tuned on resonance with an excited state of the dots, is studied by optical micro-spectroscopy.

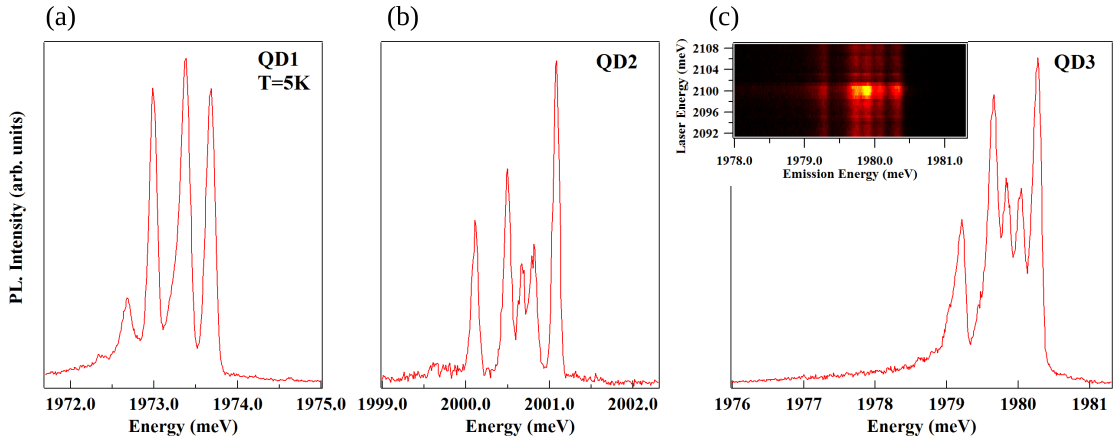

Figure II.1: PL of (a) QD1, (b) QD2 and (c) QD3 X-Cr complex at low temperature (T=5K). Inset presents the PLE map of this QD, showing a sharp quasi-resonant state for an excitation at 2100 meV.

Low temperature (T=5K) PL of the neutral exciton (X-Cr) of several QDs doped with a single Cr are reported in Fig. II.1. Four emission lines are observed as shown in QD1, with the central peak being split in some QDs, such as QD2 and QD3. Scanning with an energy tunable laser, we saw that all the peaks share a common quasi-resonant state, where all are at a maximum intensity, as highlighted in the inset of Fig. II.1(c). This is an indication that they originate from the same dot. Variations in the relative intensities of the peaks are observed in different dots. The lowest energy peak is shown as getting more intense when the splitting of the central peak get wider.

In a II-VI semiconductor, the orbital momentum of the Cr connects the spin of the atom to its local strain environment through the modification of the crystal field and the spin-orbit coupling. For biaxial strain in the (001) plane, the ground state of a Cr spin is split by a strain induced magnetic anisotropy term $\mathcal{H}_{Cr,\varepsilon_{\parallel}} = D_0 S_z^2$ (see Sec. I.3.2). It was deduced from electron paramagnetic resonance of bulk Cr-doped CdTe that D_0 is positive for compressive biaxial strain [32]. In a self-assembled CdTe/ZnTe QDs with large in-plane strain, the Cr spin energy levels are split from $|S_z = 0\rangle$ at low energy (Fig. II.2). A value of D_0 in the 1 meV range can be expected for a CdTe layer strained on a ZnTe substrate, as shown in Sec. I.3.2.

When an electron-hole pair is injected in a Cr-doped QD, the bright excitons

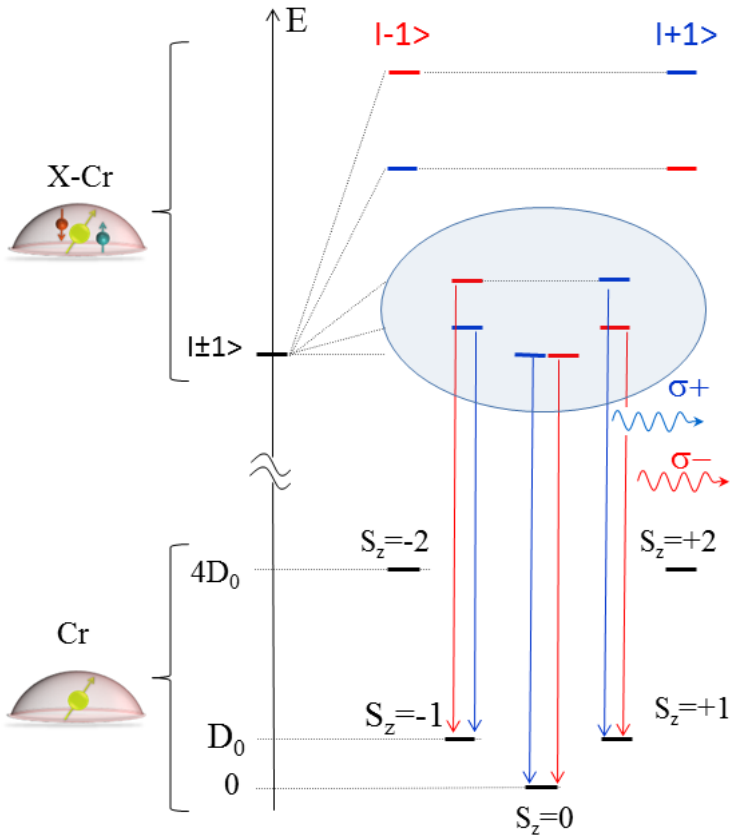

Figure II.2: Illustration of the energy levels of the ground state (Cr), the bright exciton states ($|\pm 1\rangle$) coupled to the spin of a Cr (X-Cr) and dominant PL transitions (σ+, σ-). The states $S_z = |\pm 2\rangle$ cannot be populated through thermalization, and thus their recombination channel are not shown on this schema.

are split by the exchange interaction between the spins of Cr and carriers. In flat self-assembled QDs, the heavy-holes and light-holes are separated in energy by the biaxial strain and the confinement. In a first approximation, the ground state in such QD is a pure heavy-hole (J_z=$\pm 3/2$) exciton and the exchange interaction with the Cr spin S is described by the spin Hamiltonian

$$\mathcal{H}_{c-Cr} = I_{eCr}\mathbf{S}\cdot\boldsymbol{\sigma} + I_{hCr}S_zJ_z \tag{II.1}$$

with $\boldsymbol{\sigma}$ the electron spin and J_z the hole spin operator. I_{eCr} and I_{hCr} are, respectively, the exchange integrals of the electron and the hole spins with the Cr spin. These exchange energies depend on the exchange constant of the Cr $3d$ electrons of with the CdTe carriers and on the overlap of the Cr atom with the confined carriers. Even though the exchange interaction of the Cr spin with both electron

and hole is ferromagnetic in most II-VI semiconductor [22, 23, 25], the hole-Cr interaction is supposed to be anti-ferromagnetic here. This will be further discussed in Sec. II.1.3. A typical exchange constant 4 to 5 times larger for the holes than for the electrons is also expected in CdTe [37, 38].

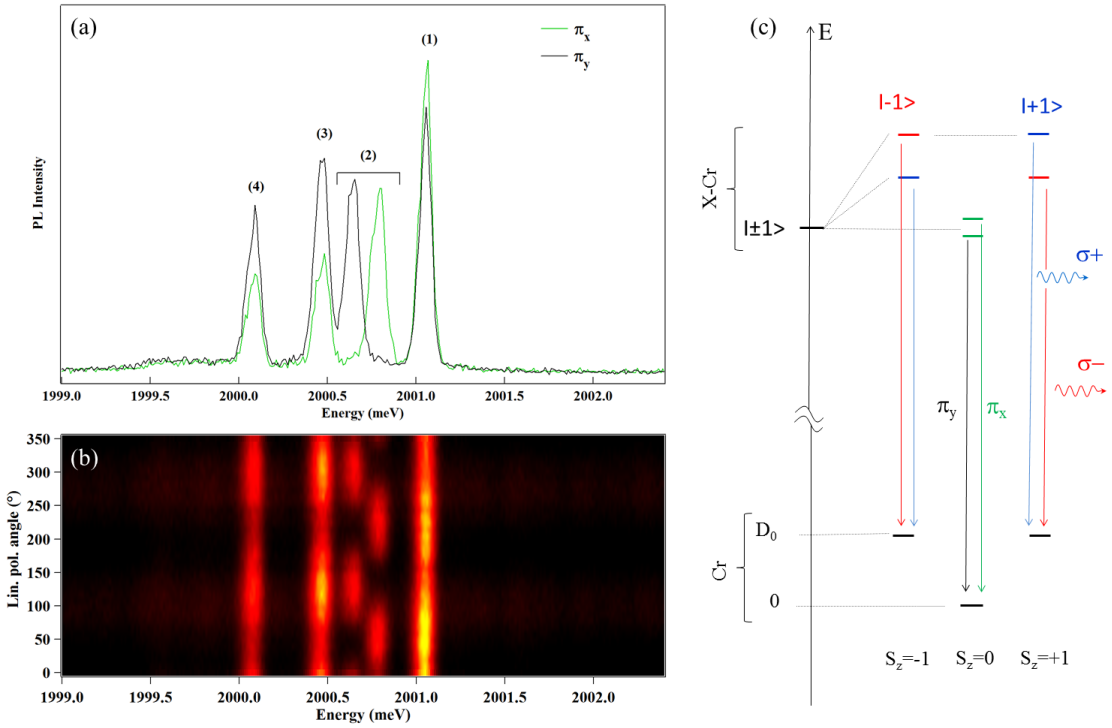

Figure II.3: (a) Low temperature PL of QD2 recorded along two orthogonal directions. (b) Linear polarization PL intensity map of QD2. The 0° polarization angle corresponds to an emission polarized along the QD cleavage axis, either 110 or $1\bar{1}0$. (c) Illustration of the energy levels of the ground state (Cr), the bright exciton states ($|\pm 1\rangle$) coupled to the spin of a Cr (X-Cr), showing the splitting of the central peak via the bright exciton coupling, and dominant PL transitions ($\sigma+$ (blue), $\sigma-$ (red) and π (green and black)).

For highly strained CdTe/ZnTe QDs with a weak hole confinement, the strain induced energy splitting of the Cr spin $D_0 S_z^2$ is much larger than the exchange energy with the confined carriers ($D_0 \gg |I_{hCr}| > |I_{eCr}|$). The exchange interaction with the exciton acts as an effective magnetic field which further splits the Cr spins states $S_z = \pm 1$ and $S_z = \pm 2$. The resulting X-Cr energy levels are presented in Fig. II.2. The exciton recombination does not affect the Cr atom and its spin is conserved during the optical transitions. Consequently, the large strain induced splitting of the Cr spin is not directly observed in the optical spectra. However, at

low temperature, the Cr spin thermalize on the low energy states S_z=0 and S_z=±1. This leads to a PL dominated by three contributions: a central line corresponding to $S_z = 0$ and the two outer lines associated with $S_z = \pm 1$ split by the exchange interaction with the carriers.

Cr-doped quantum dots exhibit a linear polarization dependence, as presented in Fig. II.3. The central line (S_z=0) is split and linearly polarized along two orthogonal directions. As in non-magnetic QDs, this results from a coupling of the two bright excitons $|\pm 1\rangle$ by (i) the short range e-h exchange interaction in the presence of valence band mixing and/or (ii) the long-range e-h exchange interaction in a QD with an in-plane shape anisotropy [39]. This anisotropic e-h exchange energy mixes the bright exciton associated with the same Cr spin state, inducing an extra splitting between them. The mixing is maximum for the central pair of bright excitons (S_z=0) which are initially degenerated. The outer lines are also slightly linearly polarized but the influence of the e-h exchange interaction is attenuated by the initial splitting of the $|\pm 1\rangle$ excitons induced by the exchange interaction with the Cr spin$S_z = \pm 1$.

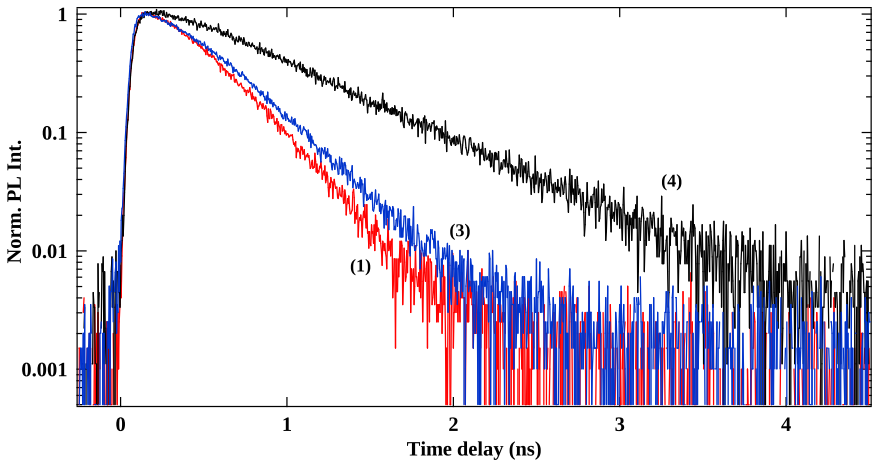

Figure II.4: Time resolved PL of QD2 taken on two exterior peaks, attributed to $|S_z = +1\rangle$ and $|S_z = -1\rangle$ (noted (1) and (3) in Fig. II.3(a)), and the lower energy one (noted (4)).

In order to identify the lower energy peak ((4) in Fig. II.3(a)), we took the time resolved photoluminescence of the emission peaks, presented in Fig. II.4. One can notice that the line (4) present a decay time about twice as long as the high energy peak. Under normal circumstances, the recombination of such a state is non-radiative. However, it is possible to observe a dark exciton recombination emitting a photon in low symmetry quantum dot [17]. Since it is initially a

forbidden transition, the relaxation will be less efficient and will thus take more time [40]. This hypothesis will be confirmed by the magneto-optical study of the dot presented in Fig. II.8 and II.12.

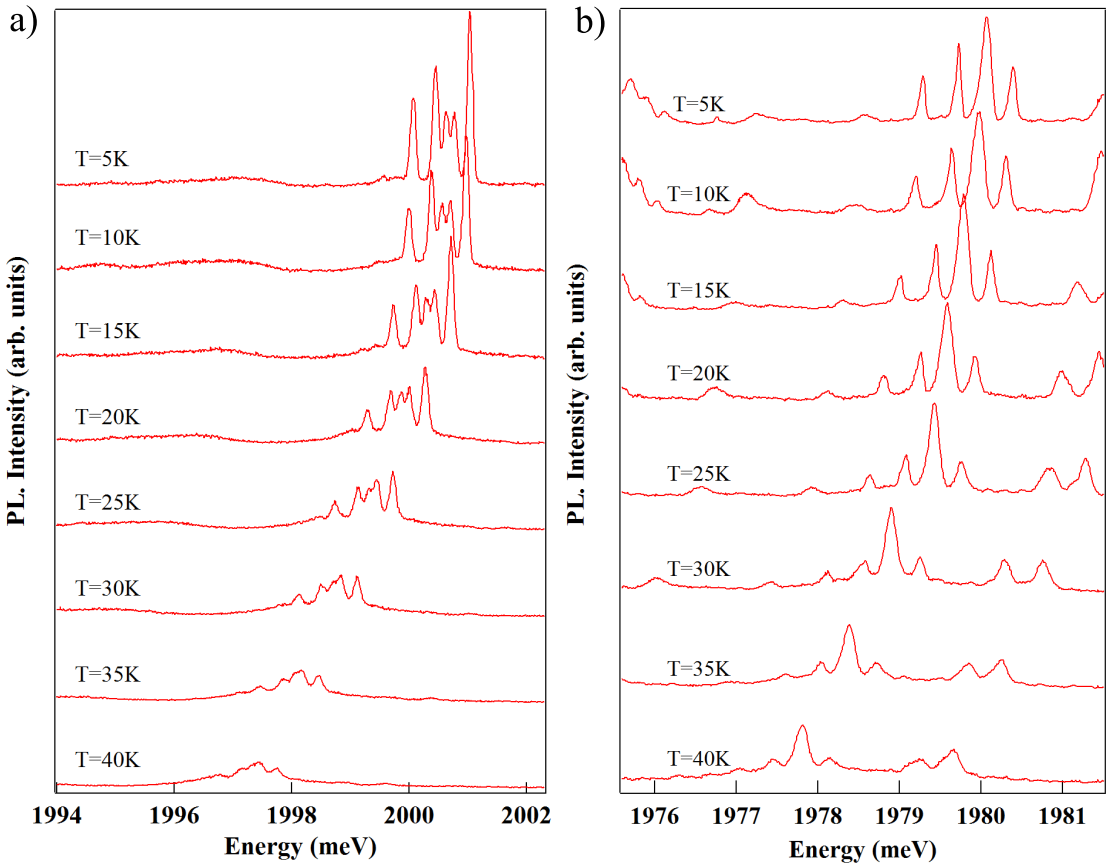

Figure II.5: Temperature evolution from T=5K to T=40K of (a) QD2 PL and (b) the PL of a QD with a good thermalisation on the low energy states (QD4). Even at 40K, $|S_z = \pm 2\rangle$ states do not appear.

Since $|\pm 2\rangle$ states do not appear on the PL because they cannot be thermally populated, one could expect to see their emission at higher temperature. Fig. II.5 presents the emission of two dots in function of the temperature. With the increase of the temperature, we observe a significant line broadening induced by the interaction with acoustic phonons. In order to keep a significant PL intensity and resolved PL lines, we limited our investigation to temperature below 50K. The figure of the emission change dramatically with the temperature. The intensity of the exterior peaks, associated with the states $S_z = |\pm 1\rangle$, fell quickly while the emission of the $S_z = |0\rangle$ stays intense until higher temperature. This is an

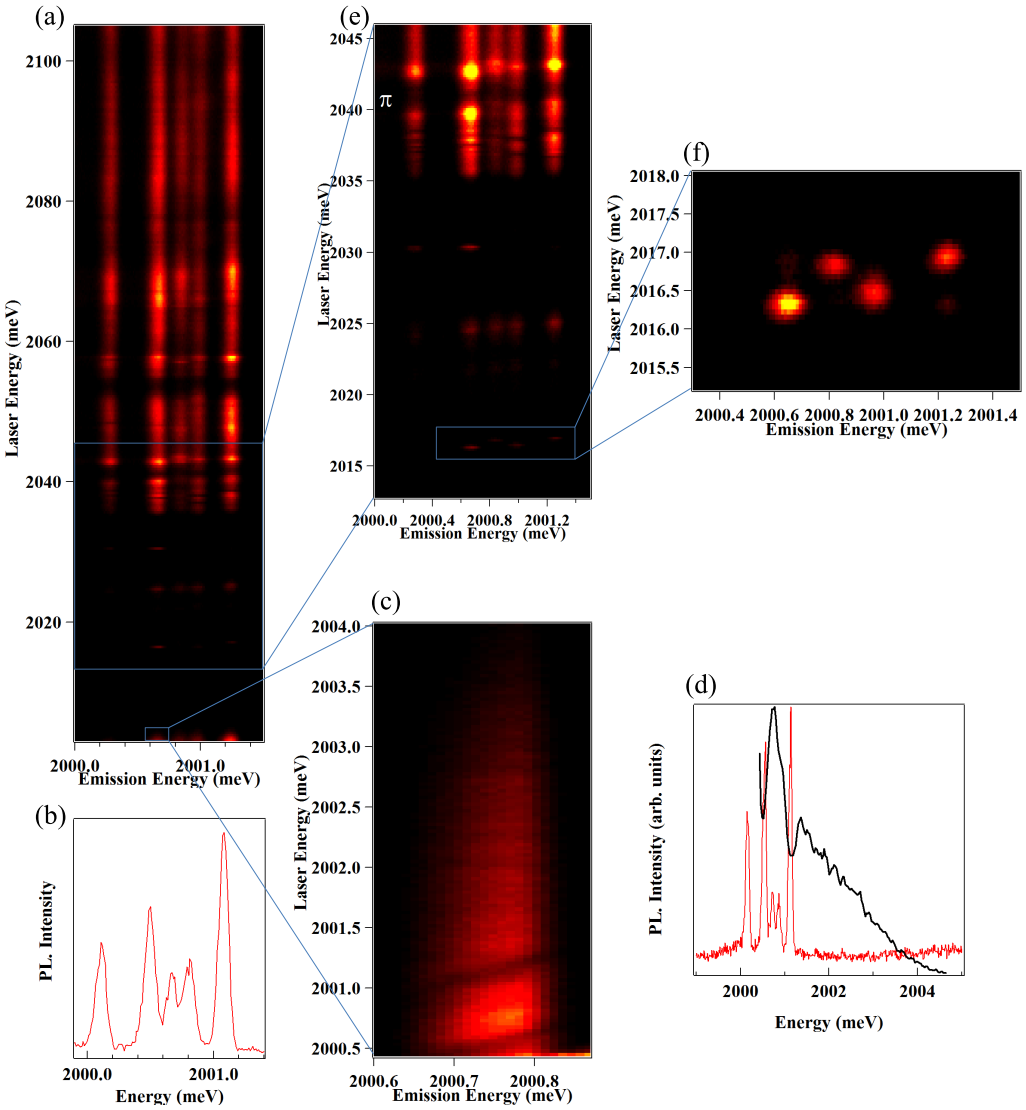

Figure II.6: (a) QD2 X-Cr PLE map in σ_{cross} polarization. Several excited states are highlighted. (b) Photoluminescence of QD2 X-Cr complex for an excitation on a quasi-resonant state (E_{laser} = 2120 meV). (c) PLE scan of the lower energy peak, taken close to the QD emission energy, showing the phonon replica taken in π detection. The emission integrated intensity in function of the laser energy is plotted in (d) (black curve) along with the PL spectra of QD2 taken in σ_{co} polarization. (e) PLE map between 2046 meV and 2013 meV presenting several excited, detecting in π. (f) Zoom in a particular excited state presented a splitting inversion, taken in π detection.

unexpected picture, since the temperature should allow the higher energy states $|\pm 1\rangle$ to be more populated by emptying the ground state, when the opposite is sawn in the experiments. Moreover, even at high temperature, the $S_z = |\pm 2\rangle$ states doesn't appears.

II.1.2 Excited states of a Cr-doped QD

In order to study the different excited states presented by a QD doped with a single Cr atom, we took the PLE of QD2 starting close to the energy of the dot's emission. Fig. II.6(a) presents the entire PLE of QD2 X-Cr complex. One can note several excited states along the scan.

The first remarkable feature of this scan is the really long luminescence of the acoustic phonon replica. As shown on the zoom in Fig. II.6(b), the probed peak continues to emit with an excitation several millielectronvolt above the excited state, remaining visible until 2004 meV. When on this band, the laser heat the sample, creating phonon in the absorption band on the dot. The first remarkable feature of this scan is the really long luminescence of the acoustic phonon replica. As shown on the zoom in Fig. II.6(b), the probed peak continues to emit with an excitation several millielectronvolt above the excited state, remaining visible until 2004 meV. When on this band, the laser heat the sample, creating phonon in the absorption band on the dot. One can also see two sharp intensity diminutions in this emission. Mapping the intensity of the phonon replica to the quantum dot spectrum (Fig. II.6(c)), it evidences that these diminutions happens when the laser is in resonance with a QD emission line. The absorption then preferentially occurs in this resonantly excited state than in the acoustic phonon band.

At higher excitation energy, several excited states appear. The lower energy one is around 2018.5 meV, zoomed in on Fig. II.6(e). The first striking feature of this peak is that, even though the studied dot contain a Cr, each of the peak here presents a slightly different resonant energy. Moreover, one can note that the order of appearance of the two central peaks seems to be reversed compared to the external ones. This phenomenon, called splitting inversion, was first observed on QDs in GaAs quantum well [41]. It has been discussed by Takagahara [39] and is likely due to the electron-hole exchange interaction.

Another excited state can be saw at 2025 meV. This one occurs on a large energy band and can be linked back to an excitation of the optical phonons. Looking at the σ polarized emission of this state (Fig. II.7(b) and (c)), we can see that the low and high energy peaks are strongly σ polarized, while the central peaks do not show dependency over circular polarization. This, once again, shows the good spin conservation of the system, as highlighted on the quasi-resonant state.

Finally, another interesting excited state appear at 2030 meV. This state presents an exchange-induced splitting different from the splitting in the quasi-resonant

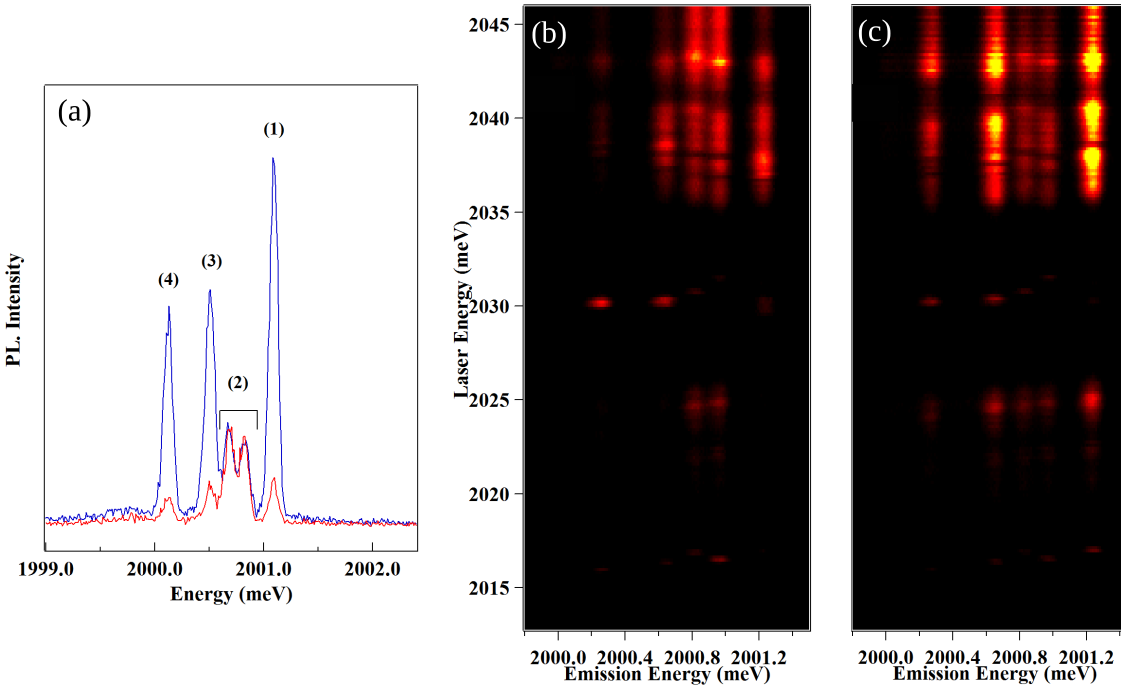

Figure II.7: (a) PL spectra of the exciton in QD2 (X-Cr) for co-circularly (blue) and cross-circularly (red) polarized excitation/detection taken on the 2120 meV quasi-resonant state. (b) - (c) PLE map between 2046 meV and 2013 meV presenting several excited states, detecting in σ_{co} (b) and σ_{cross} (c).

state. This is due to a difference in the carriers and Cr atom wavefunction overlap. One can also noticed the this state presents a stronger luminescence in σ_{cross} than in σ_{co}. It could be caused by a spin flip of the electron and hole before the recombination. By exciting the sample in a given polarization, we control the spin of the injected exciton. An emission in the opposite polarization means its spin flip before the recombination occur, leading to an exciton of the opposite spin than the one injecting and thus an emission in the opposite polarization.

II.1.3 Magneto-optics of a quantum dot doped with a single Cr

The structure of the energy levels in Cr-doped QDs is confirmed by the evolution of the PL spectra in magnetic field (up to 11T) along the growth axis, the so called Faraday configuration [42], presented in Fig. II.8. Under magnetic field, the bright exciton $X_z = \pm 1$ split, leading to a $\sigma-$ branch going at low energy and

a $\sigma+$ one going at high energy. This splitting of the excitonunder magnetic field can compensate the one induced by the exchange interaction with the Cr [43]. For QD1, this results in an anti-crossing of $|+1\rangle$ and $|-1\rangle$ excitons due to the e-h exchange interaction around B_z=6 T observed both in $\sigma+$ and $\sigma-$ polarizations (anti-crossing (2) and (3) in Fig. II.8(a)).

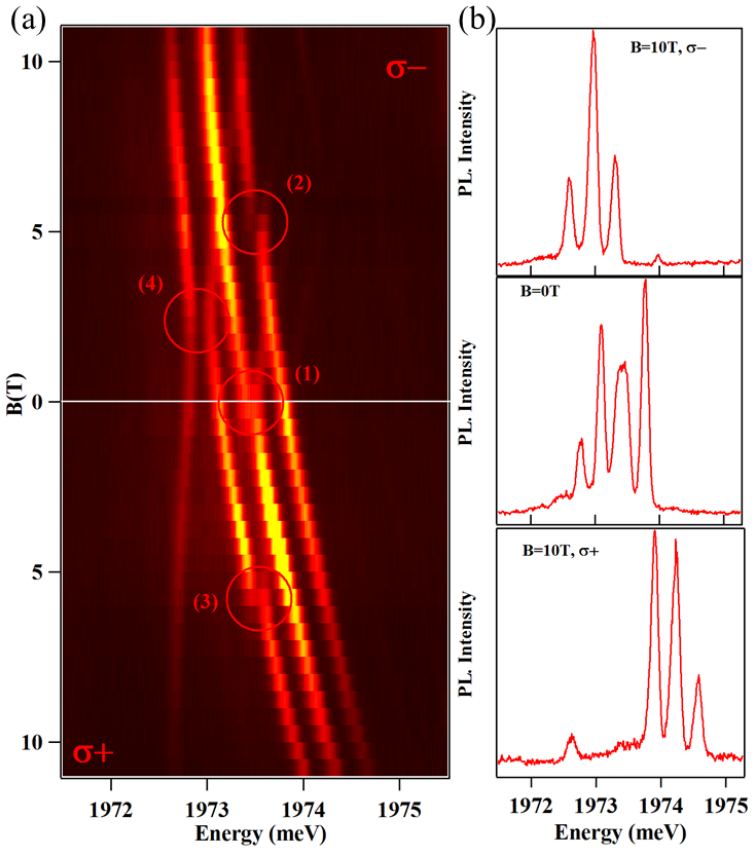

Figure II.8: (a) Circularly polarized X-Cr PL evolution under magnetic field (B_z) in QD1. Anti-crossings are highlighted and numbered. (b) QD1 X-Cr PL spectra taken at 0 and 10T for both circular polarization.

The low energy emission presented as a dark exciton in Fig. II.4 shows an anti-crossing with the bright excitons under B_z in $\sigma-$ polarization (anti-crossing (4) in Fig. II.8). As illustrated in Fig. II.12(b), this anti-crossing arises from a mixing of the bright and dark excitons interacting with the same Cr spin state. Observed in $\sigma-$ polarization, it corresponds to the mixing of the exciton states $|-1\rangle$ and $|+2\rangle$ coupled to the Cr spin $S_z = -1$. This dark/bright excitons coupling δ_{12} is induced by the e-h exchange interaction in a confining potential

of reduced symmetry (lower than C_{2v}) [44]. In such symmetry, the dark exciton acquire an in-plane dipole moment which leads to possible optical recombination at zero magnetic field [17] as observed in these QDs. The oscillator strength of this "dark exciton" increases as the initial splitting between $|-1\rangle$ and $|+2\rangle$ excitons is reduced by the magnetic field.

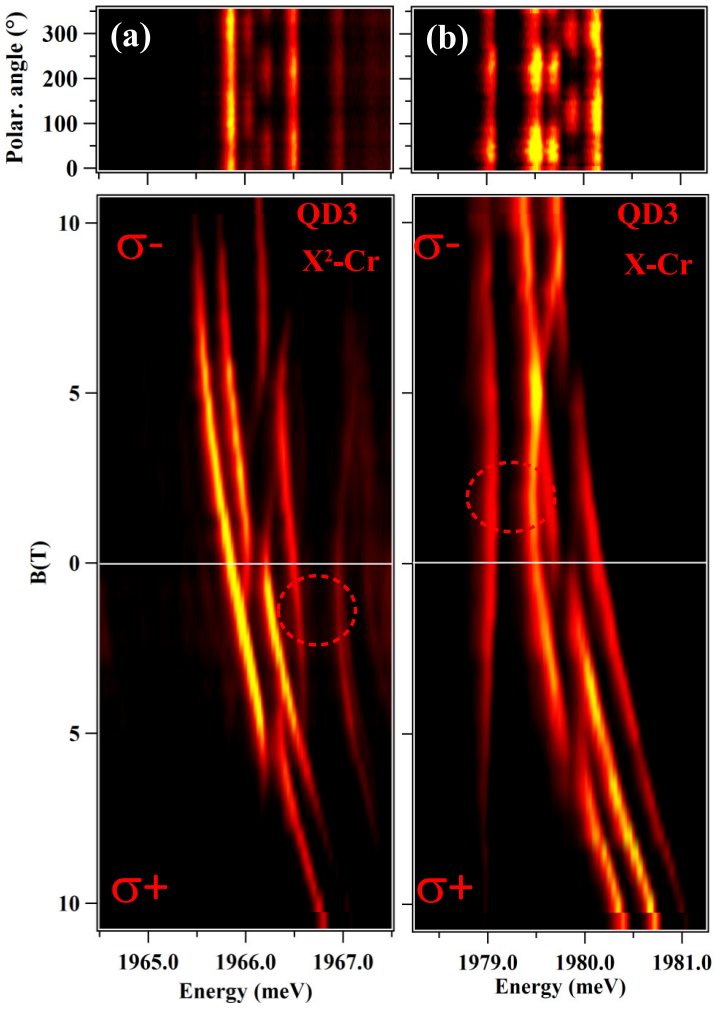

Figure II.9: Linear polarization intensity map (top panel) and intensity map of the longitudinal magnetic field dependence of the emission (bottom panel) of (a) X^2-Cr and (b) X-Cr in QD3.

To illustrate the influence of the QD symmetry on the magneto-optical properties of X-Cr, we show in Fig. II.9(b) the emission of a QD with a different strain state (QD3). For QD1, the splitting of the central peak is not clear in the PL at 0T

(Fig. II.1(a)), while two linearly polarized peaks appears clearly in QD3 spectra. This difference in emission arises from a difference in the in-plane strain of each QD [39]. The dark exciton emission is also stronger in QD2, confirming a lower symmetry than QD1.

Investigating both the biexciton and the exciton in the same Cr-doped QD, we can also analyze the impact of the carrier-Cr interaction on the fine structure of the Cr spin. The magnetic field dependency of X^2-Cr emission in QD3 is presented along with the X-Cr emission as a contour plot in Fig. II.9(a) and (b) respectively. The PL under magnetic field of X-Cr and X^2-Cr presents a mirror symmetry. In particular, the dark/bright exciton mixing observed around $B_z = 2.5$ T on the low energy side of the PL in $\sigma-$ polarization for X-Cr is observed on the high energy side in $\sigma+$ polarization for X^2-Cr (circles in Fig. II.9(a) and (b)).

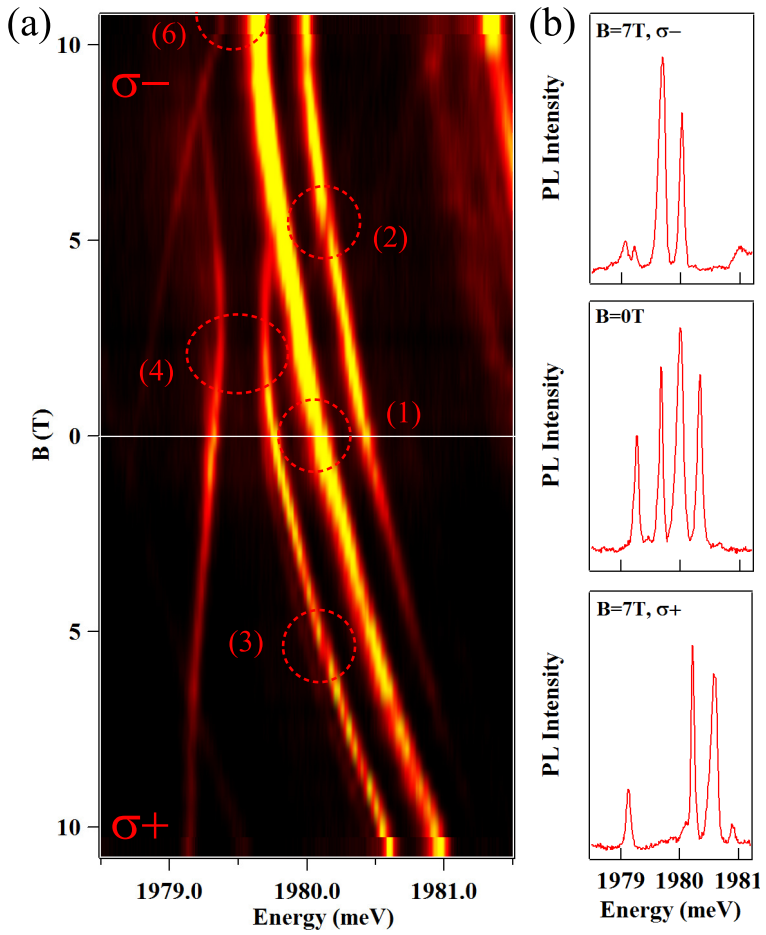

Figure II.10: (a) Evolution in magnetic field of QD4 X-Cr circularly polarized PL. (b) Highlight of the PL evolution at $B_z = 0$ T and $B_z = 7$ T in both polarization.

If one consider the ground state of X^2 as a spin-singlet (total spin 0), it cannot be split by the magnetic field or the spin interaction part of the carriers-Cr hamiltonian. The creation of two excitons in the QD cancels the exchange interaction with the Cr atom. Thus, the PL of X^2-Cr is controlled by the final state of the optical transitions, i.e. the eigenstates of X-Cr, resulting in the observed mirror symmetry in the PL spectra. However, in some of the QDs, the X^2-Cr emission slightly deviates from this simple picture: a smaller energy splitting is observed for X^2-Cr compared to X-Cr (see X-Cr and X^2-Cr in Fig. II.9). This shows that there is an interaction of X^2 with the Cr atom. It could results from a perturbation of the carriers' wave function by the interaction with the magnetic atom [45, 46] or a modification the local electric field which controls the Cr fine structure. More investigation are needed to discriminate those two hypothesis.

The evolution under magnetic field of the relative intensity of each of the QD peak gives information on the sign of the interaction between the Cr and the hole. As shown in Fig. II.2, given a polarization, each peak can be linked to a Cr spin state. As discussed earlier, applying a magnetic field lift the degeneracy between the exciton states and allow to efficiently select the polarization of the emission. For QD1, as shown in Fig. II.8, all peaks keep the same emission intensity throughout the entire map. It hints for a high spin effective temperature, mediated by out of equilibrium phonons, allowing for high energy states to be populated.

QD3, (Fig. II.9) and QD4 (Fig. II.10) presents a better thermalisation and thus shows a clearer evolution of the intensity under magnetic field. The $S_z = 0$ state is not affected by the magnetic field and remains the lower spin state for the Cr atom. Therefore, it stays populated for all values and orientations of the magnetic field. The picture is different for the exterior peaks. In the $\sigma-$ branch, the high energy peak get brighter while the low energy one disappear for $B_z \geq 8$T in QD4. The situation is opposite in the $\sigma+$ branch, where the intensity concentrate on the lower energy peak. This evolution is the same at the one found for single Mn atoms in II-VI QDs, presented in Fig. II.11. It was shown in Yoan Léger PhD thesis [11] that the $S_z = -\frac{5}{2}$ state of the Mn atom was stabilized under magnetic field. From this evolution and the polarization of the different Mn states, it was then possible to deduce that the interaction between Mn and hole was anti-ferromagnetic.

The situation of Cr is similar. Under magnetic field, the $S_z = -1$ is stabilized, becoming the lower energy state of the doublet $S_z = \pm 1$. For a magnetic field high enough for the other peak to disappear ($B_z = 8$ T in QD4), we can consider the states linked to $S_z = +1$ to be emptied and only consider the $S_z = -1$ ones. The high energy transition corresponds then to the $|S_z = -1, X_z = -1\rangle \rightarrow |S_z = -1\rangle$ on, in $\sigma-$ polarization, while the low energy peak is associate with the $|S_z = -1, X_z = +1\rangle \rightarrow |S_z = -1\rangle$ transition, in $\sigma+$ polarization. This is coherent with an anti-ferromagnetic coupling between the Cr and hole, contradicting the

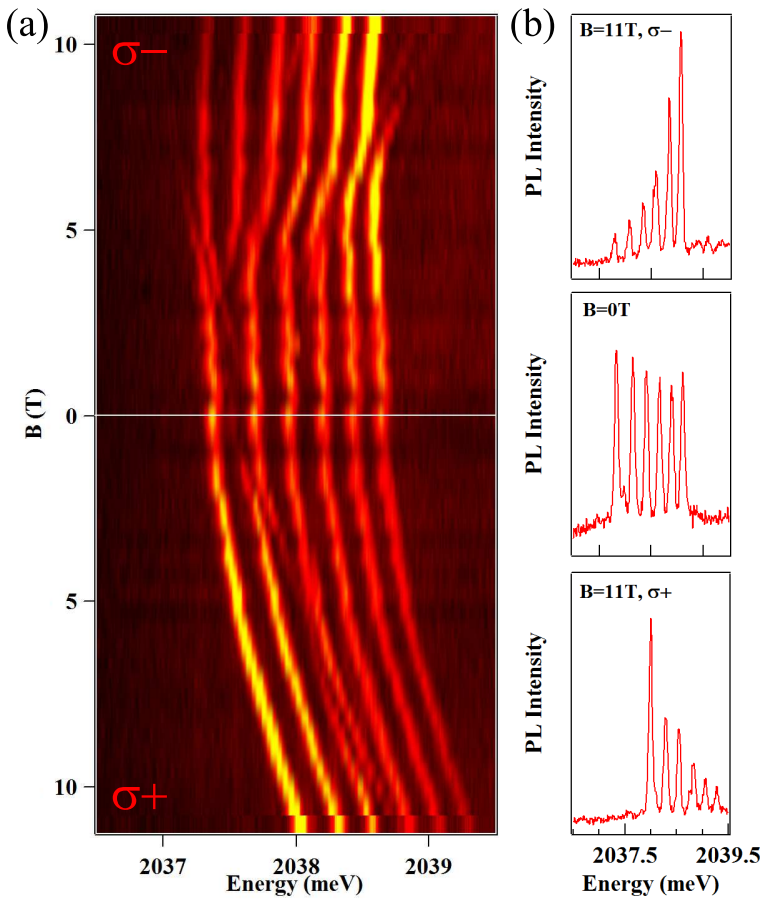

Figure II.11: (a) Evolution in magnetic field of the PL of a single Manganese atom coupled to an exciton in a II-VI QD. (b) PL spectra of the X-Mn system taken at $B_z = 0$ T and $B_z = 11$ T in both circular polarization. These experimental results are taken from Yoan Léger PhD thesis [11].

assumption made in Sec. I.2.2 and confirming the energy structure presented in Fig. II.2.

II.2 Modelization of a Cr-doped QD

We calculated the magneto-optic behaviour of Cr-doped QDs by diagonalizing the complete Hamiltonian of the e-h-Cr in self-assembled dots. This hamiltonian can be separated as follows:

$$\mathcal{H}_{X-Cr} = \mathcal{H}_{Cr,\varepsilon} + \mathcal{H}_{cCr} + \mathcal{H}_{mag} + \mathcal{H}_{eh} + \mathcal{H}_{band} + \mathcal{H}_{scat} \tag{II.2}$$

where:

$\mathcal{H}_{Cr,\varepsilon}$ describes the fine structure of the Cr atom and its dependency on local strain, as presented in Eq. I.105. It is mainly drived by D_0, the magnetic anisotropy. E, the in-plane strains, also appears in this Hamiltonian, but have to be kept small in order to model the found dots (see Fig. II.13 for the emission of a dot with a higher E).

$\mathcal{H}_{cCr}$ describes the coupling of the electron and hole with the Cr spin, depending on I_{eCr}, the exchange integral of the electron-Cr spins, and I_{hCr}, the exchange integral of the hole-Cr spins, as described in Eq. I.96.

$\mathcal{H}_{mag}$ describes the effect of an exterior magnetic field, coupled to both the Cr and carrier spins by the Zeeman terms, depending on the g-factor of each of them and the Bohr magneton μ_B, and including the diamagnetic shift of the electron-hole via the term γ.

$$\mathcal{H}_{mag} = g_{Cr}\mu_B \overrightarrow{B}.\overrightarrow{S} + g_e\mu_B \overrightarrow{B}.\overrightarrow{\sigma} + g_h\mu_B \overrightarrow{B}.\overrightarrow{J} + \gamma B^2 \tag{II.3}$$

$\mathcal{H}_{eh}$ describes the short range and long range electron-hole interaction, through the bright and dark exciton splitting δ_0, the bright exciton coupling δ_1, the dark exciton coupling δ_2 and the bright and dark exciton coupling δ_{11} and δ_{12}. All of these term are described in Eq I.54.

$\mathcal{H}_{band}$ is the band Hamiltonian. It is written $\mathcal{H}_{band} = E_g + \mathcal{H}_{VBM}$, with E_g the CdTe gap energy and $\mathcal{H}_{VBM}$ is described in Eq. I.55.

$\mathcal{H}_{scat}$ describes the perturbation of the wave function of the exciton in the initial state of the optical transition by the hole-Cr exchange interaction, controlled by the parameter η. This perturbation depends on the value of the exchange energy between the Cr spin S_z and the hole spin J_z and can be represented, using second order perturbation theory, by an effective spin Hamiltonian [36, 45, 46]

$$\mathcal{H}_{scat} = -\eta S_z^2 \tag{II.4}$$

with $\eta > 0$.

We considered the general case of QDs with a symmetry lower than C_{2v} (truncated ellipsoidal lens for instance [44]), and took into account the influence of this reduced symmetry on the valence band and on the e-h exchange interaction. The population of the X-Cr spin states split by the large magnetic anisotropy and the carriers-Cr exchange interaction is described by a spin effective temperature T_{eff}. The results of the model obtained with T_{eff}=20K, $D_0 = 2.2$ meV and an electron-Cr (hole-Cr) exchange interaction $I_{eCr} = -50$ μeV ($I_{hCr} = 250$ μeV) are reported

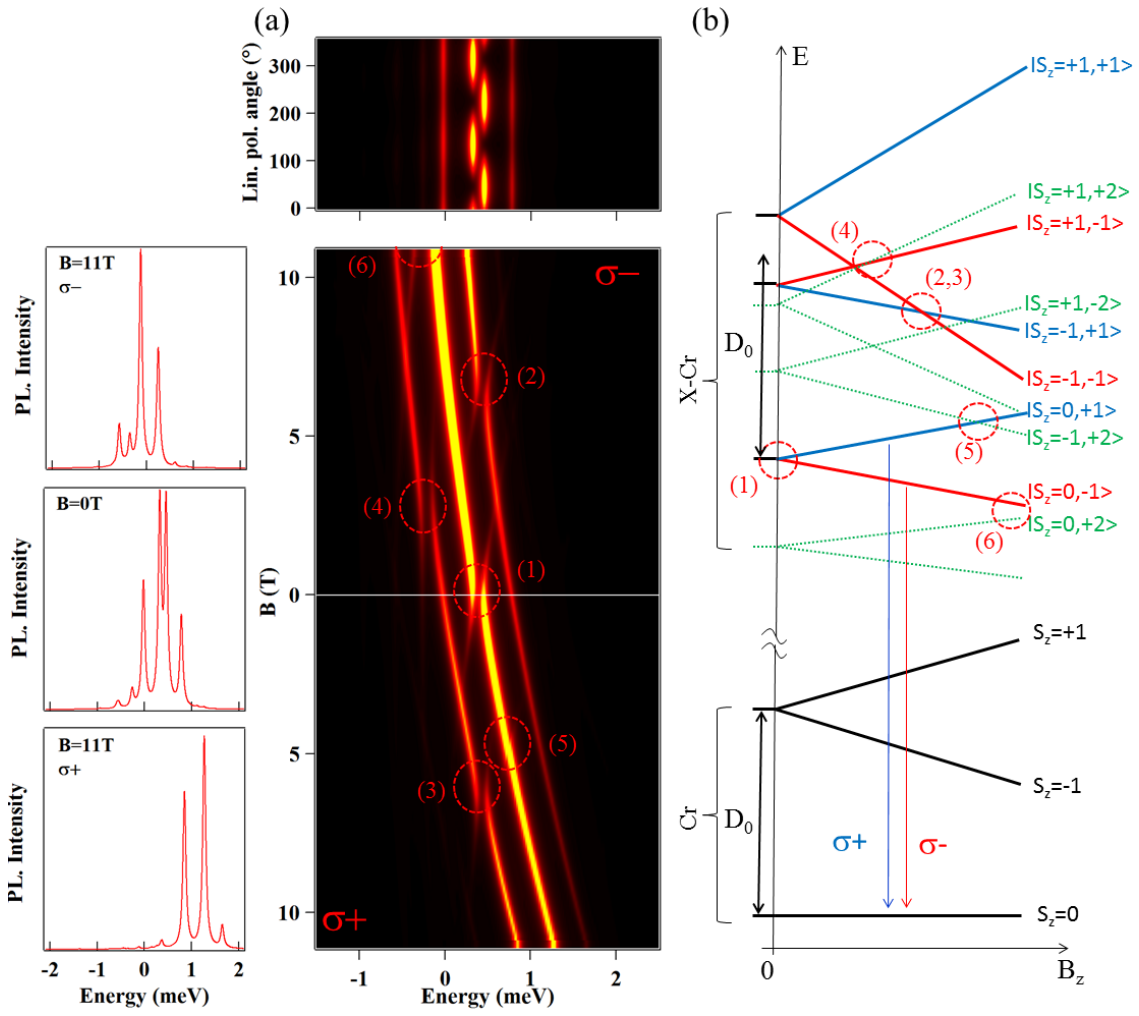

Figure II.12: (a) Up: Calculated linear polarization PL intensity map of X-Cr at zero field. The 0° polarization angle correspond to an emission polarized along the 100 axis. Down: Calculated X-Cr circularly polarized magnetic field dependency. Details of the model and parameters are listed in Tab. II.1. Corresponding anti-crossing are highlighted in same fashion as on Fig. II.8 and II.10. On the right, spectra taken for $B_z = 0$ T and $B_z = 11$ T in both circular polarization are shown. (b) Schema of the magnetic field dependency of the energy levels of the low energy Cr spin states S_z=0 and S_z=±1, and corresponding bright ($|+1\rangle$ blue, $|-1\rangle$ red) and dark ($|\pm 2\rangle$ green) X-Cr energy levels.

in Fig. II.12 (parameters not specific to Cr-doped QDs are listed in Tab. II.1). Such parameters do not aim to fit the data and are only reasonable order of magnitude

Table II.1: Values of the parameters used in the model of Cr-doped CdTe/ZnTe quantum dot presented in Fig. II.12. The value of the parameters not listed in the table is 0. The chosen values are typical for CdTe/ZnTe quantum dots and can be compared with parameters extracted from Mn-doped quantum dots [17, 36]. These values are reasonable to reproduce the emission of the QDs presented in this thesis.

I_{eCr} μeV	I_{hCr} μeV	δ_0 meV	δ_1 μeV	δ_{12} μeV	δ_{11} μeV	$\frac{\lvert Q\rvert}{\Delta_{lh}}$	$\frac{\lvert R\rvert}{\Delta_{lh}}$
-50	-250	-1	250	150	50	0.05	0.05
arg(R)	D_0 meV	g_{Cr}	g_e	g_h	γ $\mu eV/T^2$	η μeV	T_{eff} K
$-\frac{\pi}{2}$	2.2	2	-1	0.4	1.5	25	20

to qualitatively reproduce the experimental results of the PL of X-Cr at zero field and its evolution in magnetic field. The splitting of the central line at zero field (anti-crossing (1)) and the anti-crossings under magnetic field (anti-crossings (2) and (3) around B_z=6T for the Cr spin states $S_z = |+1\rangle$ and anti-crossings (4) with the dark exciton around B_z=2T) arewell reproduced by the model.

This model also predicts an anti-crossing around $B_z = 5$ T, noted (5), caused by an electron-Cr flip flop, which is not sawn on the experiments. Its position is controlled by D_0 and its intensity by I_{eCr}. However, for this anti-crossing to appear for $B_z > 11$T, a $D_0 > 3$ meV is needed, causing the $S_z = |\pm 1\rangle$ levels to be at high energy and thus giving a stronger emission intensity to the $S_z = 0$ state than the one sawn experimentally. Therefore, a low value of I_{eCr} was chosen instead. Finally, the remaining tail of an anti-crossing, labelled (6), also appears at high magnetic field in the $\sigma-$ polarization, as saw in Fig. II.10, due to the coupling a bright and a dark exciton coupled to the Cr state $|S_z = 0\rangle$.

The magnetic anisotropy D_0 cannot be precisely extracted from the PL spectra. However, for $D_0 < 2$ meV, an anti-crossing due to a VBM induced hole-Cr flip-flop between the $|-1, +2\rangle$ and the $|0, -1\rangle$ would appear below B_z=11T on the central line in $\sigma-$ polarization. Moreover, as discussed earlier, a $D_0 > 3$ meV would produce a lower PL intensity for the states $|S_z = \pm 1\rangle$. These consideration sets a D_0 in the range of 2 to 3 meV. However, even in this range, the intensity distribution of the PL cannot be perfectly reproduced: while the intensity ratio of the peaks is quite well predicted for high value of the magnetic field, the $|S_z = 0\rangle$ state still present a stronger emission at $B_z = 0$T than the one observed in the experiments. This difference in intensity may be due to out of equilibrium phonons in the sample that help populating the $|S_z = \pm 1\rangle$ states.

Our model reproduce qualitatively with enough satisfaction the data found experimentally and thus can be used to see the evolution of the emission varying different parameter. Especially, an interesting point is the influence of the anisotropy of strains on the emission. This simulation was done by applying a small magnetic anisotropy D_x along the x axis of the quantum dot and none along the y axis (D_y=0), equating to an effective E. Results of such a study are presented on Fig. II.13, (a) and (b) for the X-Cr system, and (c) and (d) for the X^c-Cr one.

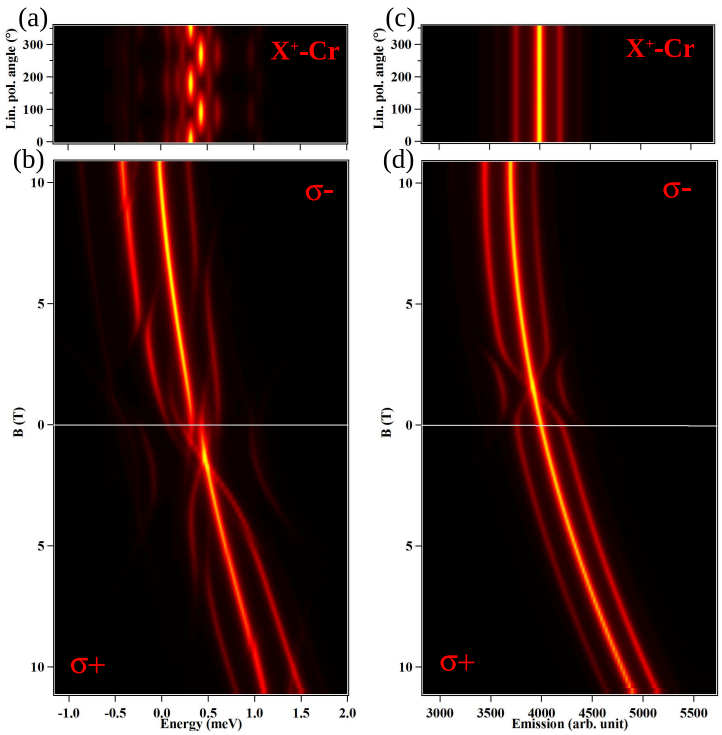

Figure II.13: For a QD with a small magnetic anisotropy along the x axis (D_x = 150 μeV, D_y = 0 μeV, D_z = 2500 μeV): (a) (resp. (c)) calculated X-Cr (resp. X^c-Cr) linear polarization PL intensity at 0T; (b) (resp. (d)) calculated X-Cr (resp. X^c-Cr) circularly polarized magnetic field dependency.

The X-Cr map in linear polarization shows a splitting of all the three peaks at 0T, when only the central peaks exhibit this behaviour in dots with a small in-plane anisotropy at the Cr position. The effect of such an anisotropy is to coupled to spin levels separated by two spin units, such as $|S_z = -1\rangle$ and $|S_z = +1\rangle$. This induce a mixing between two bright exciton states, leading to a linearly polarized emission. For a low E value, the strain induced splitting of $|S_z = \pm 1\rangle$ is high

enough to strongly reduce the mixing of the exciton states. A higher in-plane strain anisotropy is able to couple the spin level and induced the linearly polarized emission.

X^c-Cr, as said in Sec. I.1.4, is not affected by the e-h exchange interaction, and thus does not present any linear polarization dependency, as shown on Fig. II.13(c).

The evolution of the emission under magnetic field also presents different characteristics than a QD with magnetic anisotropy purely along z. Fig. II.13(b) presents the evolution in B of the X-Cr emission. One can note anti-crossings at 5 T appearing on both exterior lines in $\sigma-$ polarization, and on the low energy emission line only on $\sigma+$. These are similar to the anti-crossing (2), (3) and (4) on Fig. II.12. Around 0T, other anti-crossings appear on all the three peaks. The anti-crossing on the central peaks is the same as the anti-crossing (1) in Fig. II.12. The ones appearing on the $|S_z = \pm 1\rangle$ peaks arise from the exciton mixing via E, as evidenced by the linear polarization.

X^c-Cr in dot with high in-plane anisotropy at the Cr position also presents anti-crossing for a magnetic field around 1T, as shown in Fig. II.13(d). This anti-crossing appears when the Zeeman effect of the Cr atom compensates the electron-Chromium interaction and the hole-Chromium interaction.

II.3 Charge fluctuation of a Cr ion in the vicinity of the QDs

Some dots were found presenting a linear polarization dependency both on their central peaks and on their exterior peaks. However, such dots did not present any anti-crossing when probed under magnetic field. Results of these experiments are presented in Fig. II.14.

A common feature of all of these dots is the thin and well split X^+-Cr PL structure, shown on Fig. II.14(a) around 1949mev. X-Cr and X^2-Cr were found to exhibit a broader emission, sometime broad broad enough the three PL lines to be indistinguishable, such as QD6 presented in Fig. II.16. The linear polarization map of the QD5 PL reveals that each peak presents a linear polarization dependency (Fig. II.14(b) and (c)). The PL evolution under magnetic field of such a dot is presented in Fig. II.14(d). The diamagnetic shift is clearly visible. However, the only anti-crossings appear at $B = 9$ T for all the peaks (zoom in Fig. II.14(d)). Such anti-crossings arise from the mixing between bright and dark excitons and are characteristic of an single exciton, not coupled to a magnetic atom.

In order to get more informations on these dots, it was decided to study them applying a bias voltage. The application of an electric field was realized via a sample with a Schottky gate in the same fashion than the one in Fig. II.15(c).

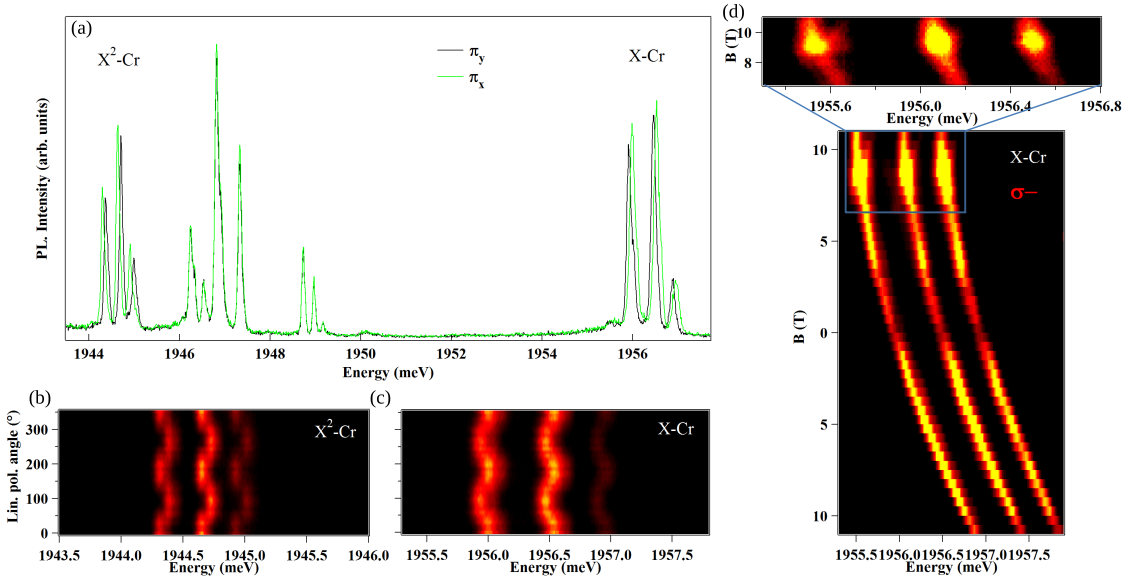

Figure II.14: (a) QD5 linearly polarized PL intensity at zero magnetic field. (b) and (c) Respectively QD6 X^2-Cr and X-Cr linear polarization PL dependence at zero magnetic field. (c) X-Cr magnetic field PL dependence on this QD. Zoom in presents anti-crossing appearing at B=9T.

The resulting map is presented in Fig. II.15(a). The first visible feature is the strong electric field dependency of the emission energy, more marked for X-Cr than for the X^c-Cr systems. The emission energy variation of the X-Cr complex occurs in a 2.9 meV range.

There is another remarkable point on these maps, evidenced on the X^+-Cr complex on the Fig. II.15(b): the splitting between each peak is changing with the applied electric field. The splitting between the high and low energy peaks varies from 0 meV for an applied bias voltage of -12V (no splitting) to 0.76 meV for 13V applied. This disappearance of the splitting for a certain bias voltage indicates that phenomena inducing an emission at three different energy can be tuned using an external electric field.

Fig. II.16 shows that, using electric field, we can manipulate the splitting of any given charged state of the QD. For all positive bias voltage between 0V and 13V, X-Cr present a broad emission containing all six peaks in linear emission, as show on Fig. II.16(a). The emission then divide into three distinct peaks, starting to appear around -1V. This is evidenced on the the PL emission on Fig. II.16(d).

This three peaks emission structure looks like a three levels system emitting at three different energies. However, the magnetic field evolution presented in

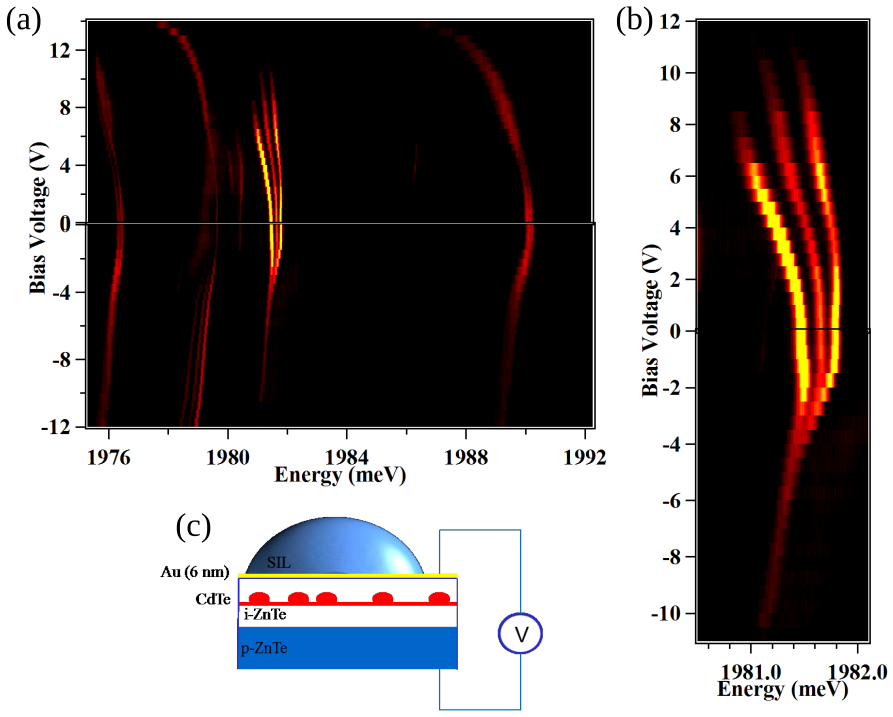

Figure II.15: (a) QD7 whole PL evolution under application of a bias voltage. (b) Zoom on X^c-Cr circular polarization PL intensity evolution under electric field. A strong stark shift is observed, as well as variation in the splitting. (c) Schema of a sample with a Schottky gate used to apply the bias voltage on the sample.

Fig. II.14(c) does not reflect the presence of a magnetic atom in the quantum dot. These features seems to arise from a single exciton trapped in a QD presenting spectral fluctuations.

Spectral fluctuations under a fluctuation of charge in the vicinity of a QD has been observed to lead to a peak broadening [47], such as observed on Fig. II.16(d), as well as spectrum jumps. For the PL to jump between three emission energies, the charge fluctuation has to be able to take three distinct charge values.

Cr in ZnTe is incorporated as Cr^{2+}, but, as shown on Fig.II.17(a), the Cr^{+} and Cr^{3+} states are also accessible [48], either by capturing an electron (Cr^{+}) or a hole (Cr^{3+}). Considering such a charge close to the QD, it can be viewed as a punctual one, since the dot is far bigger than the atom. The effect on the wave functions, presented in Fig.II.17(b)-(d), differs depending on the electrical charge of the Cr atom. The electron is well confined in CdTe/ZnTe quantum dots, while the hole is almost not confined. Because of this, the electron wave function is almost not moved by the presence of the electric, when the hole one vary more depending on

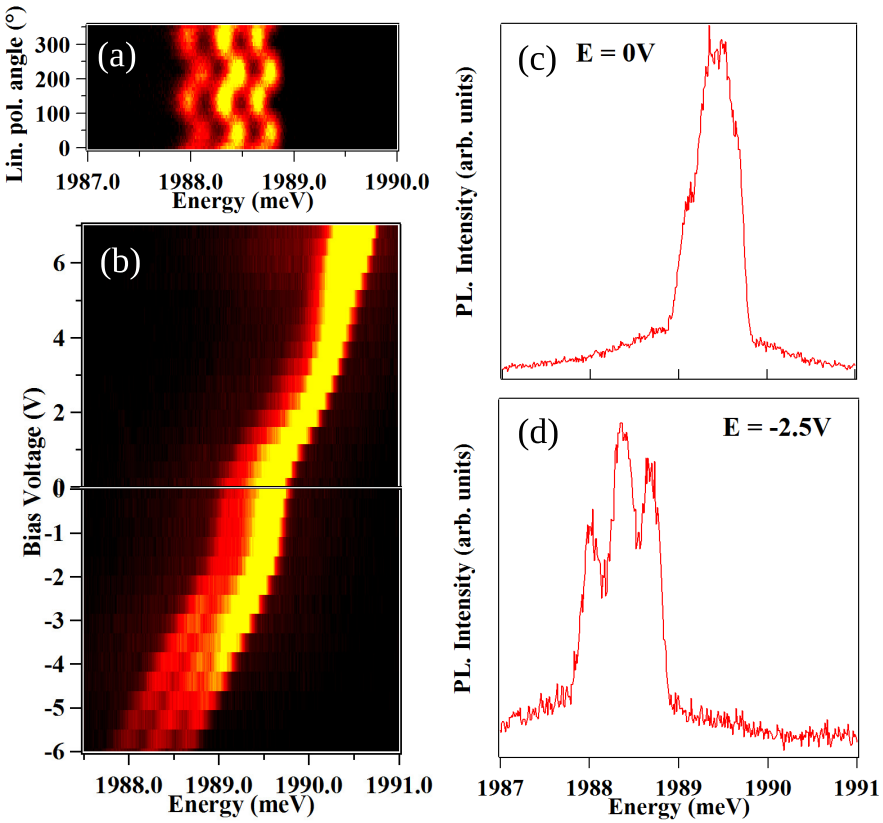

Figure II.16: All these measures were taken on QD8 X-Cr complex at low temperature. (a) PL intensity dependency in linear polarization. In order to have the best contrast, the map was taken at -2.5V bias voltage. (b) Circular PL intensity evolution in electric field. A splitting began to appear around -2V of applied bias voltage. (c)-(d) Circular PL for an applied bias voltage of, respectively, 0V and -2.5V.

the charge state of the Cr. These differences in the overlapping of wave functions lead to three different emission energies depending on the Cr charge state.

The charge variation of the Cr is of the value of the elementary charge. Considering a pure coulomb interaction between two punctual charges, for a charge at 5nm of the dot, its effect is of the same order of magnitude than the hole-Cr exchange interaction. In order to have a significant effect on the dot PL, the Cr has then to be close to it, not more than a few nanometres away.

This hypothesis is currently tested, along with the capacity for the Cr to diffuse outside the quantum dots layer.

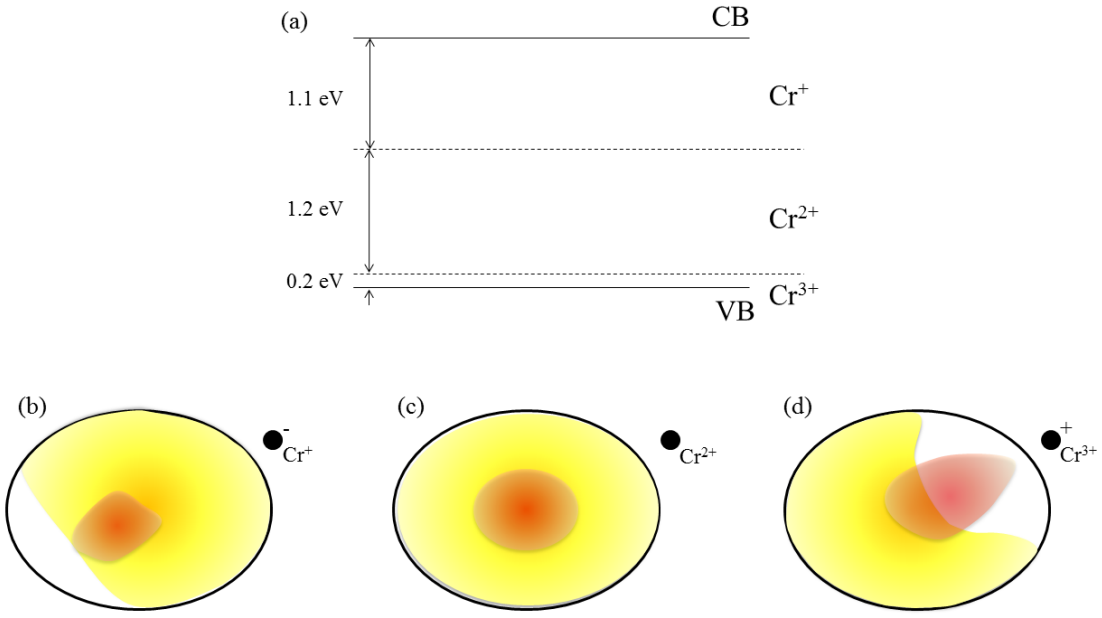

Figure II.17: (a) Cr accessible charged states in ZnTe. (b)-(d) Illustration of the effect of a punctual charge on the wavefunction of an electron (red) and a hole (yellow) in a quantum dots.

II.4 Conclusion

For the first time, a single Cr atom in a semiconductor was probed optically. The fine structure of the Cr is dominated by a magnetic anisotropy induced by strain in the plane of the QDs. The large spin to strain coupling of Cr, two orders of magnitude larger than for magnetic elements without orbital momentum (NV centers in diamond [49], Mn atoms in II-VI semiconductors [50]) suggests some possible development of coherent mechanical spin-driving of an individual magnetic atom in a nano-mechanical oscillator. This new single spin system should allow, at low temperature, to enter some coupling regimes dominated by quantum coherent dynamics not reached until now in hybrid spin-mechanical devices.

Some dots presents the same structure at 0T than dots containing a single Cr atom, but without presenting the signature of the presence of a magnetic atom under magnetic field. These dots are effected by the variation of charge of a single Cr atom in the barrier, close to the dot. Further study of the diffusion process of Cr in CdTe and ZnTe is required in order to avoid the creation of such dots.

Bibliography

[1] J. K. Furdyna, "Diluted magnetic semiconductors", Journal of Applied Physics **64**, R29–R64 (1988).

[2] E. O. Kane, "Band structure of indium antimonide", Journal of Physics and Chemistry of Solids **1**, 249–261 (1957).

[3] C. Le Gall, "Dynamics and Optical contrôl of a single spin in a Quantum Dot", Theses (Université de Grenoble, Nov. 2011).

[4] J. M. Luttinger, "Quantum theory of cyclotron resonance in semiconductors: general theory", Phys. Rev. **102**, 1030–1041 (1956).

[5] G. Bir and G. Pikus, *Symmetry and strain-induced effects in semiconductors*, Wiley (1974).

[6] J. Allègre, B. Gil, J. Calatayud, and H. Mathieu, "Deformation potentials of cdte epilayers from piezo and wavelength modulation reflectivity spectra analysis", Journal of Crystal Growth **101**, 603–607 (1990).

[7] J. M. Luttinger and W. Kohn, "Motion of electrons and holes in perturbed periodic fields", Phys. Rev. **97**, 869–883 (1955).

[8] J.-L. Basdevant and J. Dalibart, "Mécanique quantique", in (Les éditions de l'École Polytechnique, 2002) Chap. 2, p. 80.

[9] W. Wardzyński and M. Suffczyński, "Dependence of the exchange splitting in excitons on the interatomic distance", Solid State Communications **10**, 417–419 (1972).

[10] M. Zieli ński, Y. Don, and D. Gershoni, "Atomistic theory of dark excitons in self-assembled quantum dots of reduced symmetry", Phys. Rev. B **91**, 085403 (2015).

[11] Y. Léger, "Détection de spins individuels dans les boîtes quantiques magnétiques", Theses (Université Joseph-Fourier - Grenoble I, Sept. 2007).

[12] C. L. Cao, L. Besombes, and J. Fernández-Rossier, "Spin-phonon coupling in single mn-doped cdte quantum dot", Phys. Rev. B **84**, 205305 (2011).

[13]Y. Léger, L. Besombes, L. Maingault, and H. Mariette, "Valence-band mixing in neutral, charged, and Mn-doped self-assembled quantum dots", Phys. Rev. B **76**, 045331 (2007).

[14]I. Favero, G. Cassabois, C. Voisin, C. Delalande, P. Roussignol, R. Ferreira, C. Couteau, J. P. Poizat, and J. M. Gérard, "Fast exciton spin relaxation in single quantum dots", Phys. Rev. B **71**, 233304 (2005).

[15]F. Patella, S. Nufris, F. Arciprete, M. Fanfoni, E. Placidi, A. Sgarlata, and A. Balzarotti, "Tracing the two- to three-dimensional transition in the inas/gaas(001) heteroepitaxial growth", Phys. Rev. B **67**, 205308 (2003).

[16]F. Tinjod, B. Gilles, S. Moehl, K. Kheng, and H. Mariette, "II–VI quantum dot formation induced by surface energy change of a strained layer", Applied Physics Letters **82**, 4340–4342 (2003).

[17]M. Bayer, G. Ortner, O. Stern, A. Kuther, A. A. Gorbunov, A. Forchel, P. Hawrylak, S. Fafard, K. Hinzer, T. L. Reinecke, S. N. Walck, J. P. Reithmaier, F. Klopf, and F. Schäfer, "Fine structure of neutral and charged excitons in self-assembled In(Ga)As/(Al)GaAs quantum dots", Phys. Rev. B **65**, 195315 (2002).

[18]C. Tonin, R. Hostein, V. Voliotis, R. Grousson, A. Lemaitre, and A. Martinez, "Polarization properties of excitonic qubits in single self-assembled quantum dots", Phys. Rev. B **85**, 155303 (2012).

[19]L. Maingault, "Insertion d'ions magnétiques dans les boîtes quantiques de semiconducteurs II-VI", Theses (Université Joseph-Fourier - Grenoble I, Dec. 2006).

[20]J. R. Schrieffer and P. A. Wolff, "Relation between the anderson and kondo hamiltonians", Phys. Rev. **149**, 491–492 (1966).

[21]J. Gaj, R. Planel, and G. Fishman, "Relation of magneto-optical properties of free excitons to spin alignment of mn^2+ ions in cd$_{1-x}$mn$_x$te", Solid State Communications **29**, 435–438 (1979).

[22]P. Kacman, "Spin interactions in diluted magnetic semiconductors and magnetic semiconductor structures", Semicond. Sci. Technol. **16**, R25 (2001).

[23]W. Mac, A. Twardowski, and M. Demianiuk, "S,p-d exchange interaction in Cr-based diluted magnetic semiconductors", Phys. Rev. B **54**, 5528–5535 (1996).

[24]J. Blinowski, P. Kacman, and K. Majewski, "Ferromagnetism in cr-based diluted magnetic semiconductors", Journal of Crystal Growth **159**, Proceedings of the seventh international conference on II-VI compouds and devices, 972–975 (1996).

[25]M. Herbich, W. Mac, A. Twardowski, K. Ando, Y. Shapira, and M. Demianiuk, "Magnetization and exciton spectroscopy of the diluted magnetic semiconductor cd$_{1-x}$cr$_x$s", Phys. Rev. B **58**, 1912–1921 (1998).

[26] Y. Tanabe and S. Sugano, "On the absorption spectra of complex ions. I", Journal of the Physical Society of Japan **9**, 753–766 (1954).

[27] D. McClure, "Solid states physics", in, Vol. 9 (Academics, New York, 1959).

[28] J. Griffith, *The theory of transition metal ions* (Cambridge University Press, London, 1971).

[29] M. Qazzaz, G. Yang, S. Xin, L. Montes, H. Luo, and J. Furdyna, "Electron paramagnetic resonance of mn2+ in strained-layer semiconductor superlattices", Solid State Communications **96**, 405–409 (1995).

[30] M. Causa, M. Tovar, S. Oseroff, R. Calvo, and W. Giriat, "Spin-lattice coefficients of mn2+ in ii–vi compounds", Physics Letters A **77**, 473–475 (1980).

[31] C. Le Gall, L. Besombes, H. Boukari, R. Kolodka, J. Cibert, and H. Mariette, "Optical spin orientation of a single manganese atom in a semiconductor quantum dot using quasiresonant photoexcitation", Phys. Rev. Lett. **102**, 127402 (2009).

[32] J. T. Vallin and G. D. Watkins, "EPR of Cr^{2+} in II-VI lattices", Phys. Rev. B **9**, 2051–2072 (1974).

[33] M. Brousseau, *Les defauts ponctuels dans les semiconducteurs* (Les Editions de Physiques, Sept. 1988).

[34] R. D. Greenough and S. B. Palmer, "The elastic constants and thermal expansion of single-crystal CdTe", Journal of Physics D: Applied Physics **6**, 587 (1973).

[35] P. Ovartchaiyapong, K. W. Lee, B. A. Myers, and A. C. B. Jayich, "Dynamic strain-mediated coupling of a single diamond spin to a mechanical resonator", Nature Communications **5**, 4429 (2014).

[36] B. Varghese, H. Boukari, and L. Besombes, "Dynamics of a Mn spin coupled to a single hole confined in a quantum dot", Phys. Rev. B **90**, 115307 (2014).

[37] W. Mac, A. Twardowski, and M. Demianiuk, "S,p-d exchange interaction in Cr-based diluted magnetic semiconductors", Phys. Rev. B **54**, 5528–5535 (1996).

[38] M. Herbich, W. Mac, A. Twardowski, K. Ando, Y. Shapira, and M. Demianiuk, "Magnetization and exciton spectroscopy of the diluted magnetic semiconductor $Cd_{1-x}Cr_xS$", Phys. Rev. B **58**, 1912–1921 (1998).

[39] T. Takagahara, "Theory of exciton doublet structures and polarization relaxation in single quantum dots", Phys. Rev. B **62**, 16840–16855 (2000).

[40] J. McFarlane, P. A. Dalgarno, B. D. Gerardot, R. H. Hadfield, R. J. Warburton, K. Karrai, A. Badolato, and P. M. Petroff, "Gigahertz bandwidth electrical control over a dark exciton-based memory bit in a single quantum dot", Applied Physics Letters **94**, 093113 (2009).

[41]D. Gammon, E. S. Snow, B. V. Shanabrook, D. S. Katzer, and D. Park, "Fine structure splitting in the optical spectra of single GaAs quantum dots", Phys. Rev. Lett. **76**, 3005–3008 (1996).

[42]L. Besombes and H. Boukari, "Resonant optical pumping of a Mn spin in a strain-free quantum dot", Phys. Rev. B **89**, 085315 (2014).

[43]Y. Léger, L. Besombes, L. Maingault, D. Ferrand, and H. Mariette, "Geometrical effects on the optical properties of quantum dots doped with a single magnetic atom", Phys. Rev. Lett. **95**, 047403 (2005).

[44]M. Zieli ński, Y. Don, and D. Gershoni, "Atomistic theory of dark excitons in self-assembled quantum dots of reduced symmetry", Phys. Rev. B **91**, 085403 (2015).

[45]L. Besombes, Y. Leger, L. Maingault, D. Ferrand, H. Mariette, and J. Cibert, "Carrier-induced spin splitting of an individual magnetic atom embedded in a quantum dot", Phys. Rev. B **71**, 161307 (2005).

[46]A. H. Trojnar, M. Korkusinski, U. C. Mendes, M. Goryca, M. Koperski, T. Smolenski, P. Kossacki, P. Wojnar, and P. Hawrylak, "Fine structure of a biexciton in a single quantum dot with a magnetic impurity", Phys. Rev. B **87**, 205311 (2013).

[47]H. Kamada and T. Kutsuwa, "Broadening of single quantum dot exciton luminescence spectra due to interaction with randomly fluctuating environmental charges", Phys. Rev. B **78**, 155324 (2008).

[48]J. Dziesiaty, P. Peka, M. U. Lehr, A. Klimakow, S. Müller, and H.-J. Schulz, "The chromium impurity in znte: changes of the charge state detected by optical and EPR spectroscopy", ZPCH **201**, 63 (1997).

[49]A. Barfuss, J. Teissier, E. Neu, A. Nunnenkamp, and P. Maletinsky, "Strong mechanical driving of a single electron spin", Nat Phys **11**, 820 (2015).

[50]A. Lafuente-Sampietro, H. Boukari, and L. Besombes, "Strain-induced coherent dynamics of coupled carriers and Mn spins in a quantum dot", Phys. Rev. B **92**, 081305 (2015).